
PRESERVING LINEAR INVARIANTS IN ENSEMBLE FILTERING

METHODS

• Mathieu Le Provost, • Jan Glaubitz, and • Youssef Marzouk

Laboratory for Information and Decision Systems
Department of Aeronautics and Astronautics
Massachusetts Institute of Technology
Cambridge, MA, 02139, USA
{mleprovo, glaubitz, ymarz}@mit.edu

ABSTRACT

Formulating dynamical models for physical phenomena is essential for understanding the interplay between the different mechanisms, predicting the evolution of physical states, and developing effective control strategies. However, a dynamical model alone is often insufficient to address these fundamental tasks, as it suffers from model errors and uncertainties. One common remedy is to rely on data assimilation, where the state estimate is updated with observations of the true system. Ensemble filters sequentially assimilate observations by updating a set of samples over time. They operate in two steps: a forecast step that propagates each sample through the dynamical model and an analysis step that updates the samples with incoming observations. For accurate and robust predictions of dynamical systems, discrete solutions must preserve their critical invariants. While modern numerical solvers satisfy these invariants, existing invariant-preserving analysis steps are limited to Gaussian settings and are often not compatible with classical regularization techniques of ensemble filters, e.g., inflation and covariance tapering. The present work focuses on preserving linear invariants, such as mass, stoichiometric balance of chemical species, and electrical charges. Using tools from measure transport theory (Spantini *et al.*, 2022, SIAM Review), we introduce a generic class of nonlinear ensemble filters that automatically preserve desired linear invariants in non-Gaussian filtering problems. By specializing this framework to the Gaussian setting, we recover a constrained formulation of the Kalman filter. Then, we show how to combine existing regularization techniques for the ensemble Kalman filter (Evensen, 1994, J. Geophys. Res.) with the preservation of the linear invariants. Finally, we assess the benefits of preserving linear invariants for the ensemble Kalman filter and nonlinear ensemble filters.

Keywords linear invariants · measure transport · nonlinear filtering · ensemble Kalman filter

1 Introduction

Many physical and biological systems are well-described by differential equations relating the time variation of the state components to advective, diffusive, interactive, and/or reactive effects. It has long been recognized that dynamical systems possess specific properties, usually written as the conservation of invariant properties, such as mass, momentum, Hamiltonian, energy, stoichiometric balance of chemical species, and electrical charge. To produce physically admissible solutions for these differential equations, advanced numerical solvers ensure that discrete solutions mimic the critical invariants of the original system [Hairer et al., 2006].

Let us consider a state process $\{\mathbf{X}_t\}_{t \geq 0} \in \mathbb{R}^n$. We say that $\mathbf{H}: \mathbb{R}^n \rightarrow \mathbb{R}^r$ is an invariant for the state process $\{\mathbf{X}_t\}_{t \geq 0}$ if \mathbf{H} is conserved over time, i.e., for $\mathbf{X}_0 \sim \pi_{\mathbf{X}_0}$, we have $\mathbf{H}(\mathbf{X}_t) = \mathbf{H}(\mathbf{X}_0)$ for all $t \geq 0$.

Unfortunately, these numerical models are usually not sufficient to track the evolution of complex dynamical systems over time. The dynamical model might suffer from model errors, discretization errors, parameter uncertainties, and unknown forcing terms [Law and Stuart, 2015, Carrassi et al., 2018]. To produce accurate state estimates, it is therefore essential to couple these dynamical models with incoming data from physical sensors. The field of data assimilation, originally developed by the numerical weather prediction community, provides an elegant framework to combine these heterogeneous sources of information [Evensen, 1994, Asch et al., 2016]. However, these computational methods have no “intrinsic” knowledge of the invariants of the underlying dynamical system and, without proper treatment, can produce non-physical posterior state estimates, e.g., a flow field with negative mass or mass unbalance, a negative chemical concentration, a non-zero divergence flow field in incompressible fluid mechanics [Albers et al., 2019, Janjić et al., 2014]. We refer readers to [Janjić et al., 2014] for further motivations on preserving invariants in data assimilation schemes for geophysical applications. Thus, it is critical to incorporate our long-standing knowledge of physics in these data assimilation algorithms to produce physically admissible state estimates.

If the invariants of the underlying dynamical system are constant over the prior distribution, we show in Appendix A that the update of Bayes’ rule guarantees that the invariants are also constant over the posterior distribution. In this setting, violations in the invariants are entirely due to the discrete¹ treatment of the inference problem. In this work, we are interested in discrete inference algorithms that preserve this critical preservation property of Bayes’ rule.

Here, we focus on preserving linear invariants, i.e., invariants of the form $\mathbf{H}(\mathbf{X}) = \mathbf{U}_\perp^\top \mathbf{X}$ with $\mathbf{U}_\perp \in \mathbb{R}^{n \times r}$. Linear invariants are ubiquitous in engineering and science. Examples include the conservation of mass, divergence-free conditions in incompressible fluid mechanics [Kajishima et al., 2016], force balance in statics [Craig Jr and Kurdila, 2006], conservation of electrical intensities and currents in Kirchhoff’s laws, or stoichiometric balance of chemical species in chemical reactions.

Precisely, we aim to conserve linear invariants in the context of filtering. The filtering problem is a classical setting of data assimilation, where we seek to sequentially assimilate observations in our state estimate [Sanz-Alonso et al., 2023]. Let us denote by $\mathbf{X}_t \in \mathbb{R}^n$ and $\mathbf{Y}_t \in \mathbb{R}^d$ the state and observation variables at time t , respectively. In the filtering problem, we seek to estimate the so-called filtering distribution $\pi_{\mathbf{X}_t | \mathbf{Y}_{1:t} = \mathbf{y}_{1:t}^*}$, where $\mathbf{y}_1^*, \dots, \mathbf{y}_t^*$ are the realizations of the observation variables up to time t . For generic and high-dimensional state-space models, the filtering distribution is

¹We use the word “discrete” to refer to any finite representation of the inference problem, e.g., finite set of samples, finite computational grid, or even representation of operators/functions in a parametric space.

either unavailable in closed form or computationally challenging. Ensemble filters are an important class of algorithms for building Monte Carlo approximations of the filtering distribution by updating a set of samples over time [Asch et al., 2016, Carrassi et al., 2018]. They operate in two steps: the forecast step that propagates each sample through the dynamical model and the analysis step that updates the samples with incoming observations. Further details will be provided in Section 3. Importantly, the analysis step does not involve time propagation and can be treated as a static inverse problem [Le Provost et al., 2021]. Building upon the previous works [Spantini et al., 2022, Le Provost et al., 2021, 2023, Ramgraber et al., 2023], we view the analysis step as the application of a transformation (called the analysis map) $T_{\mathbf{y}_t^*}$ that maps forecast samples $\{(\mathbf{y}^{(i)}, \mathbf{x}^{(i)})\}$ from the joint forecast distribution $\pi(\mathbf{Y}_t, \mathbf{X}_t) \mid \mathbf{Y}_{1:t-1} = \mathbf{y}_{1:t-1}^*$ to samples $\{\mathbf{x}_a^{(i)}\}$ from the filtering distribution $\pi_{\mathbf{X}_t \mid \mathbf{Y}_{1:t} = \mathbf{y}_{1:t}^*}$ with $\mathbf{x}_a^{(i)} = T_{\mathbf{y}_t^*}(\mathbf{y}^{(i)}, \mathbf{x}^{(i)})$. For instance, the ensemble Kalman filter (EnKF) [Evensen, 1994] constructs an estimator for the affine linear analysis map of the Kalman filter by replacing the covariances with empirical covariances computed from the joint samples of the observations and states $\{(\mathbf{x}^{(i)}, \mathbf{y}^{(i)})\} \sim \pi(\mathbf{X}_t, \mathbf{Y}_t) \mid \mathbf{Y}_{1:t-1} = \mathbf{y}_{1:t-1}^*$ [Spantini et al., 2022, Le Provost et al., 2022].

Outside the Gaussian setting that underpins the Kalman filter and a recent extension to t -distributions [Le Provost et al., 2023], it is challenging to obtain analytical analysis maps for an arbitrary joint forecast distribution $\pi(\mathbf{X}_t, \mathbf{Y}_t) \mid \mathbf{Y}_{1:t-1} = \mathbf{y}_{1:t-1}^*$. To address these limitations, Spantini et al. [2022] introduced a framework for estimating analysis maps in non-Gaussian settings using measure transport theory. This active field of research aims at characterizing a target distribution π as the transformation of a simpler reference distribution η by a map \mathcal{S} [Villani et al., 2009, Marzouk et al., 2016, Peyré et al., 2019]. Precisely, Spantini et al. [2022] proposed a generic construction for the analysis map $T_{\mathbf{y}^*}$ using a well-chosen transport map \mathcal{S} that pushes forward the joint forecast distribution $\pi(\mathbf{X}_t, \mathbf{Y}_t) \mid \mathbf{Y}_{1:t-1} = \mathbf{y}_{1:t-1}^*$ to the $(n + d)$ -dimensional standard Gaussian reference distribution. Their methodology provides a principled generalization of the linear Kalman filter to nonlinear analysis maps, producing consistent inference for non-Gaussian filtering problems. The resulting ensemble filter is called the stochastic map filter (SMF).

As mentioned above, modern numerical solvers used in the forecast step typically preserve invariants of the dynamical system, such that violations of the invariants are due to flaws in the discrete approximation of the analysis step. Motivated by this limitation, we introduce a class of analysis maps preserving linear invariants in non-Gaussian settings. The preservation of invariants in ensemble filters can be understood in a strong sense (which this paper considers) or in a weak sense. In the strong sense, the analysis map produces posterior samples with exactly the same invariants as the prior samples. This corresponds to scenarios where the invariants are known exactly. In the weak sense, the analysis map produces posterior samples that do not strictly respect the invariants of the prior samples. This corresponds to scenarios where the value of these invariants are unknown, and we allow observations to update our belief in the invariants in a controlled manner.

In this work, we focus on preserving linear invariants which corresponds to the particular case of enforcing the linear invariants of the prior samples. The problem of enforcing constraints has been studied for the Kalman filter and the EnKF in [Simon, 2010, Amor et al., 2018, Albers et al., 2019, Gupta and Hauser, 2007, Wu et al., 2019, Zhang et al., 2020]. Different strategies have been pursued: [Simon, 2010, Albers et al., 2019] leveraged a variational formulation of the Kalman filter and the EnKF to enforce hard constraints. [Gupta and Hauser, 2007] enforced hard constraints in the Kalman filter by augmenting the observations with noiseless version of the constraints. [Prakash et al., 2010] extended this observation augmentation approach to account for soft constraints in the EnKF. [Janjić et al., 2014] used

a constrained optimization to enforce linear invariants and positivity constraints in the EnKF. [Wu et al., 2019] enforced soft constraints in the EnKF by a reweighting of the ensemble members. [Zhang et al., 2020] introduced the regularized EnKF to account for various sources of prior knowledge, e.g., hard/soft constraints and sparsity.

In contrast, the present work relies on a functional perspective and introduces a generic framework to construct Linear invariant-Preserving Analysis Maps (Lin-PAMs) in the strong sense for general—potentially non-Gaussian—settings. Precisely, consider r linear invariants for the state variable \mathbf{X} given by $\mathbf{H}: \mathbb{R}^n \rightarrow \mathbb{R}^r, \mathbf{x} \mapsto \mathbf{U}_\perp^\top \mathbf{x}$, where $\mathbf{U}_\perp \in \mathbb{R}^{r \times n}$ is a sub-unitary matrix. We introduce a class of (potentially nonlinear) analysis maps $\tilde{\mathbf{T}}_{\mathbf{y}_t^*}$ that preserve linear invariants. That is, for a pair of samples $(\mathbf{y}^{(i)}, \mathbf{x}^{(i)})$ from $\pi(\mathbf{y}_t, \mathbf{x}_t) \mid \mathbf{y}_{1:t-1} = \mathbf{y}_{1:t-1}^*$ with linear invariants $\mathbf{H}(\mathbf{x}^{(i)}) = \mathbf{C}^{(i)} \in \mathbb{R}^r$, then $\mathbf{H}(\tilde{\mathbf{T}}_{\mathbf{y}_t^*}(\mathbf{y}^{(i)}, \mathbf{x}^{(i)})) = \mathbf{C}^{(i)}$. To construct a Lin-PAM, we operate a change of variables for the analysis map between the ambient space of the observations and states and a rotated space where the linear invariants are given by the first rotated state coordinates. By performing the inference in this rotated space, one can preserve linear invariants by omitting the update of these first rotated state coordinates and finally lifting the result to the original space. Importantly, we show that by construction an empirical estimator $\hat{\mathbf{T}}_{\mathbf{y}_t^*}$ of a Lin-PAM $\tilde{\mathbf{T}}_{\mathbf{y}_t^*}$ estimated from joint forecast samples preserves linear invariants, independently of the quality of the empirical estimator $\hat{\mathbf{T}}_{\mathbf{y}_t^*}$. Section 6 specializes this construction to the Gaussian setting and recovers a projected formulation of the Kalman filter that preserves linear invariants [Amor et al., 2018]. Finally, we leverage this formulation to construct a linear invariants-preserving ensemble Kalman filter compatible with existing regularization techniques.

In Section 7, we examine different scenarios regarding preserving linear invariants by the Kalman filter and the ensemble Kalman filter. In particular, we demonstrate that the ensemble Kalman filter no longer preserves linear invariants when combined with often-used regularization techniques such as covariance inflation, localization, or tapering [Janjić et al., 2014, Asch et al., 2016]. In practice, we are often in the low-data regime, i.e., the number of samples $M = O(100)$ is small compared to the dimensions of the states and observations. Thus, these regularization techniques are critical for addressing the consequences of rank deficiency of the empirical Kalman gain, such as spurious long-range correlations, sampling errors, under-estimation of the statistics [Asch et al., 2016]. Despite their demonstrated value, these regularization techniques are known to violate linear invariants of the forecast distribution [Janjić et al., 2014]. Here, we address these shortcomings of existing regularized filters, proposing new linear invariant-preserving ones.

The contributions of this paper are:

- Section 5.2 introduces a class of analysis maps preserving linear invariants (Lin-PAMs) in the strong sense in non-Gaussian settings. We show that by construction an empirical estimator of a Lin-PAM still preserves linear invariants, independently of the quality of the estimator.
- Section 6 specializes this construction to the Gaussian case and recovers a constrained formulation of the Kalman filter [Simon, 2010].
- Section 7 clarifies results regarding the preservation of linear invariants for the **vanilla** Kalman filter and the **vanilla** ensemble Kalman filter.
- Section 8.2 demonstrates on a synthetic problem with an arbitrary number r of linear invariants that preserving invariants is most advantageous when the ensemble size M is small and the ratio of linear invariants over the state dimension r/n is large.

- Sections 8.3 and 8.4 assess the benefits of preserving linear invariants for linear/nonlinear ensemble filters on a linear advection problem and a low-dimensional chaotic system, respectively. We demonstrate on these linear/nonlinear filtering problems that preserving linear invariants leads to lower tracking error. Finally, we show that the tracking error of linear invariants can be significant for non invariant-preserving ensemble filters.

The remainder of the paper is organized as follows. Section 2 presents our notation conventions. Section 3 reviews the filtering problem and its approximation with ensemble methods. Section 4 reviews tools from measure transport to derive the formula of the analysis map. Section 5 constructs the class of linear invariant-preserving analysis maps (Lin-PAMs). Section 6 specializes the results of Section 5 to the Gaussian case. Section 7 examines settings for which the analysis map of the vanilla Kalman filter preserves linear invariants. Numerical experiments for the unconstrained/constrained ensemble Kalman filters and stochastic map filters are presented in Section 8. Concluding remarks follow in Section 9. Appendix A presents the result on the preservation of invariants in Bayesian inference problems. Details on the recursive assimilation of conditionally independent observations are discussed in Appendix B. The parameterization of the stochastic map filter is presented in Appendix C. For the sake of completeness, we provide pseudo-codes for the constrained stochastic map filter and the constrained ensemble Kalman filter, see Algorithms 1 and 2 in Appendices D and E. The code to reproduce our computational experiments is openly available at <https://github.com/mleprovost/Paper-Linear-Invariants-Ensemble-Filters>.

2 Nomenclature

In the rest of this manuscript, we use the following conventions. Serif fonts refer to random variables, e.g., \mathbf{Q} on \mathbb{R}^n or Q on \mathbb{R} . Lowercase roman fonts refer to realizations of random variables, e.g., q on \mathbb{R}^n or q on \mathbb{R} . $\pi_{\mathbf{Q}}$ denotes the probability density function for the random variable \mathbf{Q} , and $\mathbf{Q} \sim \eta$ means that the random variable \mathbf{Q} is distributed according to η . Except if otherwise stated, we assume that the probability densities have full support. The mean and covariance matrix of the random variable \mathbf{Q} are denoted by $\mu_{\mathbf{Q}}$ and $\Sigma_{\mathbf{Q}}$, respectively. The cross-covariance matrix of the random variables \mathbf{Q} and \mathbf{R} is denoted by $\Sigma_{\mathbf{Q},\mathbf{R}}$. Empirical quantities are differentiated from their asymptotic counterparts using carets above each symbol, e.g., $\hat{\mu}_{\mathbf{Q}}$. A matrix $\mathbf{U} \in \mathbb{R}^{n \times r}$ is a sub-unitary matrix if its columns are orthonormal, i.e., $\mathbf{U}^\top \mathbf{U} = \mathbf{I}_r$. A sub-unitary matrix is orthonormal if $r = n$ and $\mathbf{U}\mathbf{U}^\top = \mathbf{I}_n$.

3 Background on the filtering problem

In this work, we consider a generic state-space model given by the pair of a dynamical model and an observation model for the state process $\{\mathbf{X}_t\}_{t \geq 0}$ and the observation process $\{\mathbf{Y}_t\}_{t > 0}$. The state process $\{\mathbf{X}_t\}_{t \geq 0}$ is fully described by an initial distribution $\pi_{\mathbf{X}_0}$ and a dynamical model that propagates the state forward in time:

$$\mathbf{X}_{t+1} = \mathbf{f}(\mathbf{X}_t) + \mathbf{W}_t, \text{ for } t \geq 0, \quad (1)$$

where $\mathbf{f} : \mathbb{R}^n \rightarrow \mathbb{R}^n$ is the forward operator and the process noise $\mathbf{W}_t \in \mathbb{R}^n$ is independent of the state \mathbf{X}_t . Unfortunately, we do not typically have access to full observations of the state, instead the state process $\{\mathbf{X}_t\}_{t \geq 0}$ is only observed through an indirect and perturbed process $\{\mathbf{Y}_t\}_{t > 0}$, where the observation \mathbf{Y}_t at time t is given by the observation model

$$\mathbf{Y}_t = \mathbf{g}(\mathbf{X}_t) + \mathcal{E}_t, \text{ for } t > 0, \quad (2)$$

where $g: \mathbb{R}^n \rightarrow \mathbb{R}^d$ is the observation operator and the observation noise variable \mathcal{E}_t is independent of the state \mathbf{X}_t . We assume that no observations are collected at time $t = 0$.

We are interested in the filtering problem where we want to characterize the filtering density $\pi_{\mathbf{X}_t | \mathbf{Y}_{1:t} = \mathbf{y}_{1:t}^*}$, which describes the probability of a particular state realization at time t given all the realizations of the observation variable \mathbf{Y} up to that time [Asch et al., 2016]. The filtering density $\pi_{\mathbf{X}_t | \mathbf{Y}_{1:t} = \mathbf{y}_{1:t}^*}$ cannot be computed in closed form for generic state-space models and non-Gaussian initial state distributions. This limitation motivated the development of empirical approximations of the filtering density, presented in the next paragraph. It is important to note that through the form of the dynamical and observation models, we are making particular assumptions on the conditional independence structure of the joint distribution of the state and observation processes $\pi_{\mathbf{X}_{0:t}, \mathbf{Y}_{1:t}}$ [Carrassi et al., 2018, Evensen et al., 2022]. Indeed, we assume that the state process follows a Markov chain such that the state at time t is conditionally independent of the state realizations at previous times given the state at time $t - 1$, i.e., $\mathbf{X}_t \perp\!\!\!\perp \mathbf{X}_s | \mathbf{X}_{t-1}$ for any $s \leq t - 1$. This implies $\pi_{\mathbf{X}_t | \mathbf{x}_{1:t-1}} = \pi_{\mathbf{X}_t | \mathbf{x}_{t-1}}$. Similarly, we assume that the observation variable \mathbf{Y}_t at time t is conditionally independent of the state realizations at previous times given the state at time t , i.e., $\pi_{\mathbf{Y}_t | \mathbf{x}_{1:t}} = \pi_{\mathbf{Y}_t | \mathbf{x}_t}$. Under these conditional independence assumptions, we can factorize the joint distribution $\pi_{\mathbf{X}_{0:T}, \mathbf{Y}_{1:T}}$ as

$$\pi_{\mathbf{X}_{0:T}, \mathbf{Y}_{1:T}} = \underbrace{\pi_{\mathbf{X}_0}}_{\text{initial distribution}} \prod_{t=1}^T \underbrace{\pi_{\mathbf{Y}_t | \mathbf{x}_t}}_{\text{observation model}} \underbrace{\pi_{\mathbf{x}_t | \mathbf{x}_{t-1}}}_{\text{dynamical model}}. \quad (3)$$

From this decomposition, we derive a recursive relation to propagate the filtering distribution at time t from the filtering distribution at time $t - 1$:

$$\pi_{\mathbf{X}_t | \mathbf{Y}_{1:t}} \propto \pi_{\mathbf{Y}_t | \mathbf{x}_t} \pi_{\mathbf{x}_t | \mathbf{Y}_{1:t-1}} = \pi_{\mathbf{Y}_t | \mathbf{x}_t} \int \pi_{\mathbf{x}_t | \mathbf{x}_{t-1}} \pi_{\mathbf{x}_{t-1} | \mathbf{Y}_{1:t-1}} d\mathbf{X}_{t-1} \quad (4)$$

This recursive update operates in two steps. First, the forecast distribution $\pi_{\mathbf{x}_t | \mathbf{Y}_{1:t-1}}$ is obtained by propagating the filtering distribution $\pi_{\mathbf{x}_{t-1} | \mathbf{Y}_{1:t-1}}$ through the transition kernel $\pi_{\mathbf{x}_t | \mathbf{x}_{t-1}}$ of the dynamical model (1), i.e., $\pi_{\mathbf{x}_t | \mathbf{Y}_{1:t-1}} = \int \pi_{\mathbf{x}_t | \mathbf{x}_{t-1}} \pi_{\mathbf{x}_{t-1} | \mathbf{Y}_{1:t-1}} d\mathbf{X}_{t-1}$. This last equation is known as the Chapman-Kolmogorov equation [Asch et al., 2016, Carrassi et al., 2018]. Second, we apply Bayes' rule to condition the forecast distribution on the realization of the observation at time t , resulting in the filtering distribution at time t .

As mentioned earlier, solving analytically the filtering problem is generally infeasible outside of the linear Gaussian setting [Asch et al., 2016]. Instead, we rely on a Monte Carlo approximation of the filtering density $\pi_{\mathbf{x}_t | \mathbf{Y}_{1:t}}$ by propagating a set of M samples $\{\mathbf{x}^{(i)}\}$ over time. It has been established that particle filters — without adequate treatment — suffer from the curse of dimensionality and require an exponentially growing number of samples with the dimension of the problem [Bengtsson et al., 2008, Snyder et al., 2008, Cotter et al., 2020]. We do not consider this class of methods in this work and focus on algorithms assigning equal weights to all the samples. We call algorithms falling under this category ensemble filtering methods [Carrassi et al., 2018, Spantini et al., 2022]. These algorithms mimic the two-step recursive update of the filtering distribution presented in (4) at the sample level. In the first step, called the forecast step, each sample is propagated through the dynamical model (1). The resulting samples form a Monte Carlo approximation of the forecast distribution $\pi_{\mathbf{x}_t | \mathbf{Y}_{1:t-1}}$. In the second step, called the analysis step, we condition the forecast samples on the realization of the observation variable at time t , denoted \mathbf{y}_t^* . We use the star superscript to stress that \mathbf{y}_t^* is the observation to assimilate. To condition forecast samples on this new observation realization, we leverage the formalism of measure transport [Marzouk et al., 2016, Spantini et al., 2022]. To this end, we rely on the existence of a transformation $T_{\mathbf{y}_t^*}$, called prior-to-posterior transformation or analysis map, that transforms the joint

forecast distribution $\pi(\mathbf{y}_t, \mathbf{x}_t) \mid \mathbf{y}_{1:t-1} = \mathbf{y}_{1:t-1}^*$ into the filtering distribution $\pi_{\mathbf{x}_t} \mid \mathbf{y}_{1:t} = \mathbf{y}_{1:t}^*$. Under Gaussian assumptions on the joint forecast distribution of the states and observations, the analysis map corresponds to the celebrated Kalman filter update [Kalman, 1960, Spantini et al., 2022]. In practice, the analysis map must be approximated from samples $\{(\mathbf{y}^{(i)}, \mathbf{x}^{(i)})\}$ of the joint forecast distribution $\pi(\mathbf{y}_t, \mathbf{x}_t) \mid \mathbf{y}_{1:t-1} = \mathbf{y}_{1:t-1}^*$. For instance, the ensemble Kalman filter (EnKF) introduced by Evensen [1994] relies on a Monte Carlo approximation of the Kalman gain $\Sigma_{\mathbf{x}_t, \mathbf{y}_t} \Sigma_{\mathbf{y}_t}^{-1}$ from the joint forecast samples.

4 Background on ensemble transport methods

The goal of this section is to review triangular transport maps. In particular, we recall some of their appealing properties for conditional inference and how they can be leveraged to construct analysis maps [Spantini et al., 2022].

4.1 Overview of triangular transport methods

We start by recalling some introductory elements on triangular transport methods [Marzouk et al., 2016]. Given a target distribution with density $\pi : \mathbb{R}^m \rightarrow \mathbb{R}$, it is helpful to describe it as the transformation of a simpler reference distribution with density $\eta : \mathbb{R}^m \rightarrow \mathbb{R}$ by a map $\mathcal{S} : \mathbb{R}^m \rightarrow \mathbb{R}^m$. A bijective and differentiable map \mathcal{S} that transforms the distribution π into η is called a transport map, and we say that \mathcal{S} “pushes forward” π to η , denoted $\mathcal{S}_\# \pi = \eta$ [Marzouk et al., 2016]. The formula for the push-forward distribution $\mathcal{S}_\# \pi$ corresponds to the classical change of variables in multivariate calculus:

$$\mathcal{S}_\# \pi(\mathbf{z}) = \pi(\mathcal{S}^{-1}(\mathbf{z})) \det \nabla_{\mathbf{z}} \mathcal{S}^{-1}(\mathbf{z}) \quad (5)$$

The perspective of transport maps is appealing for sampling purposes as i.i.d. samples $\{\mathbf{z}^{(i)}\}$ from η get mapped to i.i.d. samples $\{\mathcal{S}(\mathbf{z}^{(i)})\}$ from π [Marzouk et al., 2016]. Building such transformations \mathcal{S} is the core topic of measure transport theory [Marzouk et al., 2016], classically viewed through the perspective of cost minimization [Villani et al., 2009, Peyré et al., 2019]. In this work, we take a different perspective and focus on transformations with appealing properties for Bayesian inference. Specifically, we are interested in transport maps tailored for sampling from the conditionals of a joint distribution. In the context of the analysis step of the filtering problem discussed in Section 3, we have samples from the joint forecast distribution $\pi(\mathbf{y}_t, \mathbf{x}_t) \mid \mathbf{y}_{1:t-1}^*$ and seek to generate samples from the filtering distribution $\pi_{\mathbf{x}_t} \mid \mathbf{y}_{1:t}^*$. Among the transport maps pushing forward π to η , we consider the Knothe-Rosenblatt rearrangement [Rosenblatt, 1952] defined as the unique lower triangular and strictly increasing transformation $\mathcal{S} : \mathbb{R}^m \rightarrow \mathbb{R}^m$ to facilitate conditional sampling:

$$\mathcal{S}(\mathbf{z}) = \mathcal{S}(z_1, z_2, \dots, z_m) = \begin{bmatrix} S^1(z_1) \\ S^2(z_1, z_2) \\ \vdots \\ S^m(z_1, z_2, \dots, z_m) \end{bmatrix}, \quad (6)$$

where the strict monotonicity of $S^k : \mathbb{R}^k \rightarrow \mathbb{R}$ signifies that the univariate function $\xi \mapsto S^k(\mathbf{z}_{1:k-1}, \xi)$ is strictly monotonically increasing for all z_1, z_2, \dots, z_{k-1} . The lower triangular structure of the Knothe-Rosenblatt rearrangement presents both theoretical and computational benefits. If the reference density η can be factorized, i.e., $\eta(\mathbf{z}) = \prod_{i=1}^m \eta_i(z_i)$, then Marzouk et al. [2016] showed that the univariate function $\xi \mapsto S^k(\mathbf{z}_{1:k-1}, \xi)$ resulting from fixing the first $k - 1$ entries pushes forward the conditional distribution $\pi_{\mathbf{z}_k} \mid \mathbf{z}_{1:k-1}(\xi \mid \mathbf{z}_{1:k-1})$ to the k th component of the

reference density, i.e., $S^k(\mathbf{z}_{1:k-1}, \cdot) \# \pi_{\mathbf{z}_k | \mathbf{z}_{1:k-1}}(\xi | \mathbf{z}_{1:k-1}) = \eta_k$. Once the map \mathcal{S} has been determined, one can easily represent any conditional of the target distribution. In the next section, we will show how to leverage this property to construct the analysis map. We note that monotone lower triangular transformations are also computationally attractive as the determinant of their Jacobian reduces to the product of the partial derivative of each map component with respect to its last entries. Moreover, the inversion of lower triangular transformations reduces to a sequence of univariate root finding problems [Marzouk et al., 2016]. Remarkably, the Knothe-Rosenblatt rearrangement is known in the Gaussian case (see Remark 1 below) and has recently been identified for multivariate t -distributions by Le Provost et al. [2023].

Remark 1 (The Gaussian case). *Consider $\mathbf{X} \sim \pi_{\mathbf{X}} = \mathcal{N}(\boldsymbol{\mu}, \boldsymbol{\Sigma})$ and the Cholesky factorization $\mathbf{L}^\top \mathbf{L} = \boldsymbol{\Sigma}^{-1}$. Then $\mathcal{S}(\mathbf{x}) = \mathbf{L}(\mathbf{x} - \boldsymbol{\mu})$ is the Knothe-Rosenblatt rearrangement that pushes forward $\pi_{\mathbf{X}}$ to $\eta = \mathcal{N}(\mathbf{0}_n, \mathbf{I}_n)$. The proof uses properties on linear transformations of Gaussian variables, and is omitted for brevity.*

Remark 2. *For convenience, we drop the time-dependent subscripts from the variables in the rest of this paper, since the analysis step does not involve time propagation.*

4.2 Construction of the analysis map

We now revisit the construction of the analysis map $T_{\mathbf{y}^*}$ that pushes forward the joint forecast distribution $\pi(\mathbf{Y}_t, \mathbf{X}_t) | \mathbf{Y}_{1:t-1} = \mathbf{y}_{1:t-1}^*$ to the filtering distribution $\pi_{\mathbf{X}_t | \mathbf{Y}_{1:t} = \mathbf{y}_{1:t}^*}$. In the rest of the paper, we omit the time dependence subscript of the variables as often as possible, as the analysis step involves a static Bayesian inverse problem [Spantini et al., 2022, Le Provost et al., 2022]. The joint random variable (\mathbf{Y}, \mathbf{X}) will refer to the joint forecast random variable $(\mathbf{Y}_t, \mathbf{X}_t) | \mathbf{Y}_{1:t-1} = \mathbf{y}_{1:t-1}^*$.

Consider the Knothe-Rosenblatt rearrangement \mathcal{S} that pushes forward the joint distribution of the observations and states $\pi_{\mathbf{Y}, \mathbf{X}}$ to the product reference distribution $\eta = \eta_{\mathbf{Y}} \otimes \eta_{\mathbf{X}}$ with $\eta_{\mathbf{Y}} : \mathbb{R}^d \rightarrow \mathbb{R}$ and $\eta_{\mathbf{X}} : \mathbb{R}^n \rightarrow \mathbb{R}$. From its lower triangular structure, \mathcal{S} can be partitioned in two blocks:

$$\mathcal{S}(\mathbf{y}, \mathbf{x}) = \begin{bmatrix} \mathcal{S}^{\mathbf{Y}}(\mathbf{y}) \\ \mathcal{S}^{\mathbf{X}}(\mathbf{y}, \mathbf{x}) \end{bmatrix}, \quad (7)$$

where $\mathcal{S}^{\mathbf{Y}} : \mathbb{R}^d \rightarrow \mathbb{R}^d$ and $\mathcal{S}^{\mathbf{X}} : \mathbb{R}^d \times \mathbb{R}^n \rightarrow \mathbb{R}^n$. [Baptista et al., 2020, Theorem 2.4] showed that if \mathcal{S} is lower triangular and pushes forward $\pi_{\mathbf{Y}, \mathbf{X}}$ to a product reference distribution $\eta = \eta_{\mathbf{Y}} \otimes \eta_{\mathbf{X}}$, then $\mathcal{S}^{\mathbf{X}}$ pushes forward $\pi_{\mathbf{X} | \mathbf{Y}=\mathbf{y}}$ to $\eta_{\mathbf{X}}$, i.e., $\mathcal{S}^{\mathbf{X}}(\mathbf{y}, \cdot) \# \pi_{\mathbf{X} | \mathbf{Y}=\mathbf{y}} = \eta_{\mathbf{X}}$. We note that it suffices for \mathcal{S} to be lower block triangular for this proposition to hold, i.e., $\mathcal{S}^{\mathbf{Y}}$ and $\mathcal{S}^{\mathbf{X}}$ do not need to be lower triangular. As the distributions $\eta_{\mathbf{Y}}$ and $\eta_{\mathbf{X}}$ are user-specified, one can use standard Gaussian distributions.

Once the map $\mathcal{S}^{\mathbf{X}}$ has been learned, one can easily generate samples from $\pi_{\mathbf{X} | \mathbf{Y}=\mathbf{y}^*}$ from $\eta_{\mathbf{X}}$. In practice, the learned map $\mathcal{S}^{\mathbf{X}}$ is imperfect, such that errors in the empirical map estimate $\hat{\mathcal{S}}^{\mathbf{X}}$ will be propagated in the approximation of the conditional distribution via the pullback distribution $\hat{\mathcal{S}}^{\mathbf{X}}(\mathbf{y}^*, \cdot) \# \eta_{\mathbf{X}}$. To reduce error propagation in the conditional distribution, Spantini et al. [2022] considered a composite analysis map built by partial inversion of the map $\mathcal{S}^{\mathbf{X}}$. As a consequence of the pushforward relation, we have that the conditional map $\mathbf{x} \mapsto \mathcal{S}^{\mathbf{X}}(\mathbf{y}, \mathbf{x})$ is a bijection on \mathbb{R}^n for any $\mathbf{y} \in \mathbb{R}^d$. Let (\mathbf{y}, \mathbf{x}) be a joint sample from $\pi_{\mathbf{Y}, \mathbf{X}}$. For a realization \mathbf{y}^* of the observation variable \mathbf{Y} that we want to condition on, there exists a unique element $\mathbf{x}_a \in \mathbb{R}^n$ such that $\mathcal{S}^{\mathbf{X}}(\mathbf{y}^*, \mathbf{x}_a) = \mathcal{S}^{\mathbf{X}}(\mathbf{y}, \mathbf{x})$. This element \mathbf{x}_a is precisely the posterior update of the state \mathbf{x} given the realization \mathbf{y}^* of the observation variable. See [Spantini et al., 2022, Le Provost et al., 2021] for further details. Finally, this yields the following analysis map $T_{\mathbf{y}^*} : \mathbb{R}^d \times \mathbb{R}^n \rightarrow \mathbb{R}^n$

[Spantini et al., 2022]:

$$\mathbf{T}_{\mathbf{y}^*}(\mathbf{y}, \mathbf{x}) = \mathbf{S}^{\mathbf{x}}(\mathbf{y}^*, \cdot)^{-1} \circ \mathbf{S}^{\mathbf{x}}(\mathbf{y}, \mathbf{x}), \quad (8)$$

where the notation $\mathbf{S}^{\mathbf{x}}(\mathbf{y}^*, \cdot)^{-1}$ denotes the inversion of the map $\mathbf{x} \mapsto \mathbf{S}^{\mathbf{x}}(\mathbf{y}^*, \mathbf{x})$ for fixed $\mathbf{y}^* \in \mathbb{R}^d$. We conclude this section by connecting the Kalman filter and the SMF to the analysis map of (8) in Remarks 3 and 4.

Remark 3 (Connection with the Kalman filter). *Let's consider two random variables $\mathbf{X} \in \mathbb{R}^n$ and $\mathbf{Y} \in \mathbb{R}^d$ such that (\mathbf{Y}, \mathbf{X}) is jointly Gaussian, i.e.,*

$$\begin{bmatrix} \mathbf{Y} \\ \mathbf{X} \end{bmatrix} \sim \mathcal{N} \left(\begin{bmatrix} \boldsymbol{\mu}_{\mathbf{X}} \\ \boldsymbol{\mu}_{\mathbf{Y}} \end{bmatrix}, \begin{bmatrix} \boldsymbol{\Sigma}_{\mathbf{Y}} & \boldsymbol{\Sigma}_{\mathbf{X},\mathbf{Y}}^\top \\ \boldsymbol{\Sigma}_{\mathbf{X},\mathbf{Y}} & \boldsymbol{\Sigma}_{\mathbf{X}} \end{bmatrix} \right). \quad (9)$$

Then for $\mathbf{y} \in \mathbb{R}^d$, $\pi_{\mathbf{X}|\mathbf{Y}=\mathbf{y}} = \mathcal{N}(\boldsymbol{\mu}_{\mathbf{X}|\mathbf{Y}=\mathbf{y}}, \boldsymbol{\Sigma}_{\mathbf{X}|\mathbf{Y}=\mathbf{y}})$ with $\boldsymbol{\mu}_{\mathbf{X}|\mathbf{Y}=\mathbf{y}} = \boldsymbol{\mu}_{\mathbf{X}} + \boldsymbol{\Sigma}_{\mathbf{X},\mathbf{Y}}\boldsymbol{\Sigma}_{\mathbf{Y}}^{-1}(\mathbf{y} - \boldsymbol{\mu}_{\mathbf{Y}})$ and $\boldsymbol{\Sigma}_{\mathbf{X}|\mathbf{Y}=\mathbf{y}} = \boldsymbol{\Sigma}_{\mathbf{X}} - \boldsymbol{\Sigma}_{\mathbf{X},\mathbf{Y}}\boldsymbol{\Sigma}_{\mathbf{Y}}^{-1}\boldsymbol{\Sigma}_{\mathbf{X},\mathbf{Y}}^\top$. Let $\mathbf{L}_{\mathbf{X}|\mathbf{Y}=\mathbf{y}}\mathbf{L}_{\mathbf{X}|\mathbf{Y}=\mathbf{y}}^\top = \boldsymbol{\Sigma}_{\mathbf{X}|\mathbf{Y}=\mathbf{y}}$ be the Cholesky factorization of $\boldsymbol{\Sigma}_{\mathbf{X}|\mathbf{Y}=\mathbf{y}}$. Then $\mathbf{S}^{\mathbf{x}}(\mathbf{y}, \mathbf{x}) = \mathbf{L}_{\mathbf{X}|\mathbf{Y}=\mathbf{y}}(\mathbf{x} - \boldsymbol{\mu}_{\mathbf{X}|\mathbf{Y}=\mathbf{y}})$. By applying (8), we get $\mathbf{T}_{\mathbf{y}^*}(\mathbf{y}, \mathbf{x}) = \mathbf{x} - \boldsymbol{\Sigma}_{\mathbf{X},\mathbf{Y}}\boldsymbol{\Sigma}_{\mathbf{Y}}^{-1}(\mathbf{y} - \mathbf{y}^*)$, recovering the analysis map of the Kalman filter as noted by Spantini et al. [2022]. Thus, (8) corresponds to a generalization of the Kalman filter for non-Gaussian joint distribution of the observations and states $\pi_{\mathbf{Y},\mathbf{X}}$.

Remark 4 (The stochastic map filter). *The SMF introduced in [Spantini et al., 2022] builds an estimator $\hat{\mathbf{S}}^{\mathbf{x}}$ for $\mathbf{S}^{\mathbf{x}}$ from joint forecast samples of the states and observations. The estimator $\hat{\mathbf{S}}^{\mathbf{x}}$ is based on a parsimonious expansions of radial basis functions estimated by solving decoupled and convex optimization problems. The filtering samples are obtained by applying the estimated analysis map of (8) from $\hat{\mathbf{S}}^{\mathbf{x}}$ to the joint forecast samples. Thus, the stochastic map filter can be viewed as a nonlinear generalization of the ensemble Kalman filter.*

5 Linear invariant-preserving analysis maps (Lin-PAMs)

In this section, we propose a new methodology for constructing analysis maps that preserve linear invariants of the state. Consider the linear invariants $\mathbf{H}(\mathbf{x}) = \mathbf{U}_\perp^\top \mathbf{x}$. We will design an analysis map $\mathbf{T}_{\mathbf{y}^*}$ that pushes forward $\pi_{\mathbf{Y},\mathbf{X}}$ to $\pi_{\mathbf{X}|\mathbf{Y}=\mathbf{y}^*}$ while ensuring the invariant \mathbf{H} is preserved, i.e., $\mathbf{H}(\mathbf{T}_{\mathbf{y}^*}(\mathbf{y}, \mathbf{x})) = \mathbf{H}(\mathbf{x})$ for all $(\mathbf{y}, \mathbf{x}) \in \mathbb{R}^d \times \mathbb{R}^n$. We call an analysis map verifying this property a linear invariant-preserving analysis map (Lin-PAM). Our approach works for arbitrary nonlinear analysis map and non-Gaussian joint distribution of the observations and states $\pi_{\mathbf{Y},\mathbf{X}}$. To this end, we assume that the matrix $\mathbf{U}_\perp \in \mathbb{R}^{n \times r}$ has rank r . Furthermore, without loss of generality (see Remark 5 below), we assume that \mathbf{U}_\perp is a sub-unitary matrix, i.e., \mathbf{U}_\perp has orthonormal columns.

Remark 5. *Consider a linear constraint $\mathbf{U}_\perp^\top \mathbf{x} = \mathbf{C}_\perp \in \mathbb{R}^r$, where \mathbf{U}_\perp^\top is not necessarily a sub-unitary matrix. We can then use a thin QR factorization $\mathbf{U}_\perp = \mathbf{Q}_\perp \mathbf{R}_\perp$, where $\mathbf{Q}_\perp \in \mathbb{R}^{n \times r}$ is sub-unitary and $\mathbf{R}_\perp \in \mathbb{R}^{r \times r}$ is lower triangular [Golub and Van Loan, 2013], to rewrite the linear constraint as $\mathbf{Q}_\perp^\top \mathbf{x} = \mathbf{R}_\perp^{-\top} \mathbf{C}_\perp \in \mathbb{R}^r$. Notably, \mathbf{Q}_\perp^\top is a sub-unitary matrix.*

Based on the orthonormality of \mathbf{U}_\perp , we can uniquely decompose the state $\mathbf{x} \in \mathbb{R}^n$ as

$$\mathbf{x} = \mathbf{U}_\perp \mathbf{U}_\perp^\top \mathbf{x} + (\mathbf{I} - \mathbf{U}_\perp \mathbf{U}_\perp^\top) \mathbf{x} = \mathbf{U}_\perp \mathbf{x}_\perp \oplus \mathbf{U}_\parallel \mathbf{x}_\parallel. \quad (10)$$

where $\mathbf{x}_\perp = \mathbf{U}_\perp^\top \mathbf{x} \in \mathbb{R}^r$ and $\mathbf{x}_\parallel = \mathbf{U}_\parallel^\top \mathbf{x} \in \mathbb{R}^{n-r}$. Furthermore, the matrix \mathbf{U}_\parallel is such that the columns of $\mathbf{U} = [\mathbf{U}_\perp, \mathbf{U}_\parallel] \in \mathbb{R}^{n \times n}$ form an orthonormal basis of \mathbb{R}^n . In practice, one can use a QR factorization of \mathbf{U}_\perp to build \mathbf{U}_\parallel . Thus, we have $\mathbf{x} = \mathbf{U}[\mathbf{x}_\perp; \mathbf{x}_\parallel]$, or, equivalently, $[\mathbf{x}_\perp; \mathbf{x}_\parallel] = \mathbf{U}^{-1} \mathbf{x} = \mathbf{U}^\top \mathbf{x}$.

Equation (10) is pivotal in our construction of Lin-PAMs. It allows us to reformulate the problem of building analysis maps preserving linear invariants $\mathbf{H}(\mathbf{x}) = \mathbf{U}_\perp^\top \mathbf{x}$ as building an analysis map preserving the state components in the span of \mathbf{U}_\perp . The rest of this section is organized as follows. Section 5.1 formulates the analysis map of (8) in the rotated space given by the change of variables $(\mathbf{Y}, \mathbf{X}) \mapsto (\mathbf{Y}, [\mathbf{U}_\perp, \mathbf{U}_\parallel]^\top \mathbf{X})$. Section 5.2 leverages this formulation to propose a formulation for Lin-PAMs expressed in the original space of the states and observations.

5.1 Formulation of the analysis map in the rotated space

In this section, we apply the change of coordinates $(\mathbf{Y}, \mathbf{X}) \mapsto (\mathbf{Y}, [\mathbf{U}_\perp, \mathbf{U}_\parallel]^\top \mathbf{X}) = (\mathbf{Y}, \mathbf{X}_\perp, \mathbf{X}_\parallel)$ and express the analysis map of (8) in the rotated space. The distribution $\pi_{\mathbf{X}_\perp, \mathbf{X}_\parallel}$ is given by the pushforward of $\pi_{\mathbf{X}}$ by the linear transformation \mathbf{U} , i.e., $\pi_{\mathbf{X}_\perp, \mathbf{X}_\parallel} = \mathbf{U}_\# \pi_{\mathbf{X}}$. Using the push forward formula (5), we have

$$\pi_{\mathbf{X}_\perp, \mathbf{X}_\parallel}(\mathbf{x}_\perp, \mathbf{x}_\parallel) = \pi_{\mathbf{X}}(\mathbf{U}[\mathbf{x}_\perp; \mathbf{x}_\parallel]) \det \nabla(\mathbf{U}[\mathbf{x}_\perp; \mathbf{x}_\parallel]) = \pi_{\mathbf{X}}(\mathbf{U}_\perp \mathbf{U}_\perp^\top \mathbf{x} + \mathbf{U}_\parallel \mathbf{U}_\parallel^\top \mathbf{x}) = \pi_{\mathbf{X}}(\mathbf{x}). \quad (11)$$

Thus, we have the following factorization of $\pi_{\mathbf{Y}, \mathbf{X}}$:

$$\pi_{\mathbf{Y}, \mathbf{X}}(\mathbf{y}, \mathbf{x}) = \pi_{\mathbf{Y}, \mathbf{X}_\perp, \mathbf{X}_\parallel}(\mathbf{y}, \mathbf{x}_\perp, \mathbf{x}_\parallel) = \pi_{\mathbf{Y}}(\mathbf{y}) \pi_{\mathbf{X}_\perp | \mathbf{Y}}(\mathbf{x}_\perp | \mathbf{y}) \pi_{\mathbf{X}_\parallel | \mathbf{Y}, \mathbf{X}_\perp}(\mathbf{x}_\parallel | \mathbf{y}, \mathbf{x}_\perp) \quad (12)$$

Let us now consider the Knothe-Rosenblatt rearrangement $\mathcal{S}: \mathbb{R}^d \times \mathbb{R}^r \times \mathbb{R}^{n-r}$ that pushes forward $\pi_{\mathbf{Y}, \mathbf{X}_\perp, \mathbf{X}_\parallel}$ to the product of standard Gaussian references $\eta_{\mathbf{Y}} \otimes \eta_{\mathbf{X}_\perp} \otimes \eta_{\mathbf{X}_\parallel}$, where $\eta_{\mathbf{Y}}, \eta_{\mathbf{X}_\perp}, \eta_{\mathbf{X}_\parallel}$ is defined on $\mathbb{R}^d, \mathbb{R}^r, \mathbb{R}^{n-r}$, respectively. We denote it as $\mathcal{S}_\# \pi_{\mathbf{Y}, \mathbf{X}_\perp, \mathbf{X}_\parallel} = \eta_{\mathbf{Y}} \otimes \eta_{\mathbf{X}_\perp} \otimes \eta_{\mathbf{X}_\parallel}$. From its lower triangular structure, we can partition \mathcal{S} as

$$\mathcal{S}(\mathbf{y}, \mathbf{x}_\perp, \mathbf{x}_\parallel) = \begin{bmatrix} \mathcal{S}^{\mathcal{Y}}(\mathbf{y}) \\ \mathcal{S}^{\mathcal{X}_\perp}(\mathbf{y}, \mathbf{x}_\perp) \\ \mathcal{S}^{\mathcal{X}_\parallel}(\mathbf{y}, \mathbf{x}_\perp, \mathbf{x}_\parallel) \end{bmatrix}, \quad (13)$$

where $\mathcal{S}^{\mathcal{Y}}: \mathbb{R}^d \rightarrow \mathbb{R}^d$, $\mathcal{S}^{\mathcal{X}_\perp}: \mathbb{R}^d \times \mathbb{R}^r \rightarrow \mathbb{R}^r$, and $\mathcal{S}^{\mathcal{X}_\parallel}: \mathbb{R}^d \times \mathbb{R}^r \times \mathbb{R}^{n-r} \rightarrow \mathbb{R}^{n-r}$. From the lower block structure of \mathcal{S} and [Baptista et al., 2020, Theorem 2.4], we have the following relations between the conditionals of $\pi_{\mathbf{Y}, \mathbf{X}_\perp, \mathbf{X}_\parallel}$ and the marginals of η :

$$\begin{aligned} \mathcal{S}^{\mathcal{Y}}_\# \pi_{\mathbf{Y}} &= \eta_{\mathbf{Y}}, \\ \mathcal{S}^{\mathcal{X}_\perp}_\# \pi_{\mathbf{X}_\perp | \mathbf{Y}} &= \eta_{\mathbf{X}_\perp}, \\ \mathcal{S}^{\mathcal{X}_\parallel}_\# \pi_{\mathbf{X}_\parallel | \mathbf{Y}, \mathbf{X}_\perp} &= \eta_{\mathbf{X}_\parallel} \end{aligned} \quad (14)$$

Let \mathbf{y}^* be a realization of the observation variable \mathbf{Y} . Using the relations in (14), we proceed as follows to sample from the conditional distribution $\pi_{\mathbf{X} | \mathbf{Y}=\mathbf{y}^*}$, or equivalently $\pi_{\mathbf{X}_\perp, \mathbf{X}_\parallel | \mathbf{Y}=\mathbf{y}^*}$. Let $(\mathbf{y}, \mathbf{x}_\perp, \mathbf{x}_\parallel)$ be a joint sample from $\pi_{\mathbf{Y}, \mathbf{X}_\perp, \mathbf{X}_\parallel}$. Following the derivation of the analysis map in Section 4.2, we generate samples from $\pi_{\mathbf{X}_\perp | \mathbf{Y}=\mathbf{y}^*}$ by seeking the solution $\mathbf{x}_{\perp, a} \in \mathbb{R}^r$ of

$$\mathcal{S}^{\mathcal{X}_\perp}(\mathbf{y}^*, \mathbf{x}_{\perp, a}) = \mathcal{S}^{\mathcal{X}_\perp}(\mathbf{y}, \mathbf{x}_\perp). \quad (15)$$

Formally, we therefore get the analysis map $\mathbf{T}_{\mathbf{y}^*}^\perp: \mathbb{R}^d \times \mathbb{R}^r \rightarrow \mathbb{R}^r$ that pushes forward $\pi_{\mathbf{Y}, \mathbf{X}_\perp}$ to $\pi_{\mathbf{X}_\perp | \mathbf{Y}=\mathbf{y}^*}$ as

$$\mathbf{T}_{\mathbf{y}^*}^\perp(\mathbf{y}, \mathbf{x}_\perp) = \mathcal{S}^{\mathcal{X}_\perp}(\mathbf{y}^*, \cdot)^{-1} \circ \mathcal{S}^{\mathcal{X}_\perp}(\mathbf{y}, \mathbf{x}_\perp). \quad (16)$$

Then we generate samples from $\pi_{\mathbf{X}_\parallel | \mathbf{y}^*, \mathbf{x}_{\perp, a}}$ by seeking the solution $\mathbf{x}_{\parallel, a} \in \mathbb{R}^{n-r}$ of

$$\mathcal{S}^{\mathcal{X}_\parallel}(\mathbf{y}^*, \mathbf{x}_{\perp, a}, \mathbf{x}_{\parallel, a}) = \mathcal{S}^{\mathcal{X}_\parallel}(\mathbf{y}, \mathbf{x}_\perp, \mathbf{x}_\parallel). \quad (17)$$

Similar to (16), we write the analysis map $\mathbf{T}_{\mathbf{y}^*, \mathbf{x}_{\perp, a}}^{\parallel} : \mathbb{R}^d \times \mathbb{R}^r \times \mathbb{R}^{n-r} \rightarrow \mathbb{R}^{n-r}$ that pushes forward $\pi_{\mathbf{y}, \mathbf{x}_{\parallel}, \mathbf{x}_{\perp}}$ to $\pi_{\mathbf{x}_{\parallel} | \mathbf{y}=\mathbf{y}^*, \mathbf{x}_{\perp}=\mathbf{x}_{\perp, a}}$ as

$$\mathbf{T}_{\mathbf{y}^*, \mathbf{x}_{\perp, a}}^{\parallel}(\mathbf{y}, \mathbf{x}_{\perp}, \mathbf{x}_{\parallel}) = \mathbf{S}^{\mathbf{x}_{\parallel}}(\mathbf{y}^*, \mathbf{T}_{\mathbf{y}^*}^{\perp}(\mathbf{y}, \mathbf{x}_{\perp}), \cdot)^{-1} \circ \mathbf{S}^{\mathbf{x}_{\parallel}}(\mathbf{y}, \mathbf{x}_{\perp}, \mathbf{x}_{\parallel}). \quad (18)$$

Thus, the analysis map $\mathbf{T}_{\mathbf{y}^*} : \mathbb{R}^d \times \mathbb{R}^n \rightarrow \mathbb{R}^n$ formulated in the original space that pushes forward $\pi_{\mathbf{y}, \mathbf{x}}$ to $\pi_{\mathbf{x} | \mathbf{y}=\mathbf{y}^*}$ is

$$\mathbf{T}_{\mathbf{y}^*}(\mathbf{y}, \mathbf{x}) = \begin{bmatrix} \mathbf{U}_{\perp} & \mathbf{U}_{\parallel} \end{bmatrix} \begin{bmatrix} \mathbf{x}_{\perp, a} \\ \mathbf{x}_{\parallel, a} \end{bmatrix} = \mathbf{U}_{\perp} \mathbf{T}_{\mathbf{y}^*}^{\perp}(\mathbf{y}, \mathbf{U}_{\perp}^{\top} \mathbf{x}) + \mathbf{U}_{\parallel} \mathbf{T}_{\mathbf{y}^*, \mathbf{x}_{\perp, a}}^{\parallel}(\mathbf{y}, \mathbf{U}_{\perp}^{\top} \mathbf{x}, \mathbf{U}_{\parallel}^{\top} \mathbf{x}). \quad (19)$$

Notably, (19) provides an alternative formulation for the analysis map of (8) by building analysis maps $\mathbf{T}_{\mathbf{y}^*}^{\perp}$ and $\mathbf{T}_{\mathbf{y}^*, \mathbf{x}_{\perp, a}}^{\parallel}$ in the spaces spanned by the columns of \mathbf{U}_{\perp} and \mathbf{U}_{\parallel} . We stress that (19) and (8) are strictly equivalent as (19) relies on the factorization of $\pi_{\mathbf{y}, \mathbf{x}}$ into $\pi_{\mathbf{y}} \pi_{\mathbf{x}_{\perp} | \mathbf{y}=\mathbf{y}^*} \pi_{\mathbf{x}_{\parallel} | \mathbf{x}_{\perp}, \mathbf{y}}$ instead of $\pi_{\mathbf{y}} \pi_{\mathbf{x} | \mathbf{y}}$ for (8). Interestingly, (19) proposes to perform the inference by first rotating the state along the columns of \mathbf{U} , then performing the inference for \mathbf{x}_{\perp} followed by \mathbf{x}_{\parallel} , and finally lifting the result to the original space. The idea of performing inference in a different coordinate system has been previously exploited by [Le Provost et al., 2021, 2022]. These works used likelihood-informed dimension reduction of the observations and states to perform inference in the identified low-informative subspace with low-dimensional linear/nonlinear analysis maps.

5.2 Preserving the linear invariants in the rotated space

We stress that there is no reason for the analysis map of (19) to preserve the linear invariants $\mathbf{H}(\mathbf{x}) = \mathbf{U}_{\perp}^{\top} \mathbf{x}$ in generating the posterior samples from $\pi_{\mathbf{x} | \mathbf{y}}$. The state decomposition (10) suggests that preserving $\mathbf{H}(\mathbf{x})$ corresponds to generating posterior samples from $\pi_{\mathbf{x} | \mathbf{y}=\mathbf{y}^*, \mathbf{x}_{\perp}=\mathbf{x}_{\perp, a}}$. To do so, we modify the analysis map of (19) by omitting the update of \mathbf{x}_{\perp} . This is equivalent to constrain the analysis map $\tilde{\mathbf{T}}_{\mathbf{y}^*}^{\perp}$ to be the identity, i.e., $\tilde{\mathbf{T}}_{\mathbf{y}^*}^{\perp}(\mathbf{y}, \mathbf{x}_{\perp}) = \mathbf{x}_{\perp}$. Thus, we obtain the constrained analysis map $\tilde{\mathbf{T}}_{\mathbf{y}^*}^{\parallel}$ as

$$\tilde{\mathbf{T}}_{\mathbf{y}^*}^{\parallel}(\mathbf{y}, \mathbf{x}_{\perp}, \mathbf{x}_{\parallel}) = \mathbf{S}^{\mathbf{x}_{\parallel}}(\mathbf{y}^*, \mathbf{x}_{\perp}, \cdot)^{-1} \circ \mathbf{S}^{\mathbf{x}_{\parallel}}(\mathbf{y}, \mathbf{x}_{\perp}, \mathbf{x}_{\parallel}). \quad (20)$$

We note that the second argument of $\mathbf{S}^{\mathbf{x}_{\parallel}}$ is \mathbf{x}_{\perp} in the constrained formulation instead of $\mathbf{T}_{\mathbf{y}^*}^{\perp}(\mathbf{y}, \mathbf{x}_{\perp})$ in (18). Finally, the analysis map $\tilde{\mathbf{T}}_{\mathbf{y}^*}$ formulated in the original space preserving the invariant $\mathbf{H}(\mathbf{x}) = \mathbf{U}_{\perp}^{\top} \mathbf{x}$ reads

$$\begin{aligned} \tilde{\mathbf{T}}_{\mathbf{y}^*}(\mathbf{y}, \mathbf{x}) &= \mathbf{U}_{\perp} \tilde{\mathbf{T}}_{\mathbf{y}^*}^{\perp}(\mathbf{y}, \mathbf{U}_{\perp}^{\top} \mathbf{x}) + \mathbf{U}_{\parallel} \tilde{\mathbf{T}}_{\mathbf{y}^*}^{\parallel}(\mathbf{y}, \mathbf{U}_{\perp}^{\top} \mathbf{x}, \mathbf{U}_{\parallel}^{\top} \mathbf{x}) \\ &= \mathbf{U}_{\perp} \mathbf{U}_{\perp}^{\top} \mathbf{x} + \mathbf{U}_{\parallel} \tilde{\mathbf{T}}_{\mathbf{y}^*}^{\parallel}(\mathbf{y}, \mathbf{U}_{\perp}^{\top} \mathbf{x}, \mathbf{U}_{\parallel}^{\top} \mathbf{x}). \end{aligned} \quad (21)$$

(21) and (20) form the cornerstone of the Lin-PAM methodology. In practice, an empirical estimator $\hat{\mathbf{T}}_{\mathbf{y}^*}^{\parallel}$ for the constrained analysis map $\tilde{\mathbf{T}}_{\mathbf{y}^*}^{\parallel}$ of (20) is built at each assimilation cycle from joint forecast samples $\{\mathbf{y}^{(i)}, \mathbf{x}^{(i)}\}$ of $\pi_{(\mathbf{y}_t, \mathbf{x}_t) | \mathbf{y}_{1:t-1}=\mathbf{y}_{1:t-1}^*}$. Then, we obtain the resulting constrained estimator $\hat{\mathbf{T}}_{\mathbf{y}^*}$ for the Lin-PAM $\tilde{\mathbf{T}}_{\mathbf{y}^*}$ of (21) by replacing $\tilde{\mathbf{T}}_{\mathbf{y}^*}^{\parallel}$ with $\hat{\mathbf{T}}_{\mathbf{y}^*}^{\parallel}$. Remark 6 shows that an empirical estimator $\hat{\mathbf{T}}_{\mathbf{y}^*}$ of a Lin-PAM still preserves linear invariants. Remark 7 discusses the construction of Lin-PAM of (21) when the linear invariants are constant over the prior.

We refer readers to Figure 1 for an overview of the unconstrained and constrained analysis maps presented in this section. In Appendix D, we provide a pseudo-code for the constrained stochastic map filter (ConsSMF) that performs the constrained inference of (21) from samples $\{(\mathbf{y}^{(i)}, \mathbf{x}^{(i)})\}$ of $\pi_{\mathbf{y}, \mathbf{x}}$. The ConsSMF transforms a set of forecast samples to filtering samples by assimilating the realization \mathbf{y}^* of the observation variable while preserving the linear invariants of the forecast samples. See Appendix C or [Spantini et al., 2022] for more details on the estimation of the

Knothe-Rosenblatt rearrangement—underpinning the stochastic map filters used in this work—that pushes forward the joint forecast distribution $\pi_{(\mathbf{Y}_t, \mathbf{X}_t) | \mathbf{Y}_{1:t-1} = \mathbf{y}_{1:t-1}^*}$ to the standard Gaussian distribution.

Remark 6 (An empirical estimator of a Lin-PAM preserves linear invariants). *Let $\widehat{\mathbf{T}}_{\mathbf{y}^*}^{\parallel}$ be an empirical estimator for the constrained analysis map $\widetilde{\mathbf{T}}_{\mathbf{y}^*}^{\parallel}$ of (20), and $\widehat{\mathbf{T}}_{\mathbf{y}^*}$ be the resulting estimator of the Lin-PAM $\widetilde{\mathbf{T}}_{\mathbf{y}^*}$ of (21). In practice, the estimator $\widehat{\mathbf{T}}_{\mathbf{y}^*}^{\parallel}$ is imperfect as we estimate it from samples $\{(\mathbf{y}^{(i)}, \mathbf{x}^{(i)})\}$ of an approximation of the joint forecast distribution $\pi_{(\mathbf{Y}_t, \mathbf{X}_t) | \mathbf{Y}_{1:t-1} = \mathbf{y}_{1:t-1}^*}$, and the realization \mathbf{y}_t^* to assimilate can originate from an approximation of the observation distribution $\pi_{\mathbf{Y}_t}$. Independently of these discrepancies and the quality of the estimator $\widehat{\mathbf{T}}_{\mathbf{y}^*}^{\parallel}$ for $\widetilde{\mathbf{T}}_{\mathbf{y}^*}^{\parallel}$, an empirical estimator $\widehat{\mathbf{T}}_{\mathbf{y}^*}$ preserves linear invariants. To prove this, we introduce the class of transformations $\mathcal{T}_{\text{LinP}} = \{\mathbf{T}: \mathbb{R}^d \times \mathbb{R}^n \rightarrow \mathbb{R}^n | \mathbf{T}(\mathbf{y}, \mathbf{x}) = \mathbf{U}_{\perp} \mathbf{U}_{\perp}^{\top} \mathbf{x} + \mathbf{U}_{\parallel} \mathbf{K}(\mathbf{y}, \mathbf{x}), \text{ with } \mathbf{K}: \mathbb{R}^d \times \mathbb{R}^n \rightarrow \mathbb{R}^{n-r}\}$. By noting that any estimator $\widehat{\mathbf{T}}_{\mathbf{y}^*}$ belongs to $\mathcal{T}_{\text{LinP}}$ (with $\mathbf{K}(\mathbf{y}, \mathbf{x}) = \widehat{\mathbf{T}}_{\mathbf{y}^*}^{\parallel}(\mathbf{y}, \mathbf{U}_{\perp}^{\top} \mathbf{x}, \mathbf{U}_{\parallel}^{\top} \mathbf{x})$) and that elements of $\mathcal{T}_{\text{LinP}}$ preserve the linear invariants $\mathbf{H}(\mathbf{x}) = \mathbf{U}_{\perp}^{\top} \mathbf{x}$, we obtain the desired result.*

Remark 7 (Treatment of constant linear invariants over the prior). *Assume that the linear invariants are constant over the prior $\pi_{\mathbf{X}}$, i.e., $\mathbf{U}_{\perp}^{\top} \mathbf{x} = \mathbf{C} \in \mathbb{R}^r$ for any realization $\mathbf{x} \in \mathbb{R}^n$ of \mathbf{X} . Thus, the prior $\pi_{\mathbf{X}}$ is not supported on \mathbb{R}^n but on the affine space $\{\mathbf{x} \in \mathbb{R}^n | \mathbf{U}_{\perp}^{\top} \mathbf{x} = \mathbf{C}\}$. This remark explains how to adapt the construction of Lin-PAM of (21) to this setting. Let $\mathbf{x} \in \mathbb{R}^n$ be a realization of \mathbf{X} . From the state decomposition (10), we have $\mathbf{x} = \mathbf{U}_{\perp} \mathbf{C} + \mathbf{U}_{\parallel} \mathbf{x}_{\parallel}$ with $\mathbf{x}_{\parallel} \in \mathbb{R}^{n-r}$. The distribution $\pi_{\mathbf{U}_{\perp}^{\top} \mathbf{X}}$ becomes a point mass centered at \mathbf{C} , i.e., $\pi_{\mathbf{U}_{\perp}^{\top} \mathbf{X}}(\mathbf{x}_{\perp}) = \pi_{\mathbf{X}_{\perp}}(\mathbf{x}_{\perp}) = \delta(\mathbf{C} - \mathbf{x}_{\perp})$, where δ denotes the Dirac delta distribution. Thus, we can omit the rotated state variable \mathbf{X}_{\perp} from the analysis and operate on the reduced joint space $(\mathbf{Y}, \mathbf{U}_{\parallel}^{\top} \mathbf{X}) = (\mathbf{Y}, \mathbf{X}_{\parallel})$. We define the reduced map $\mathbf{S}_{\text{reduced}}^{\mathbf{x}_{\parallel}}$ pushing forward $\pi_{\mathbf{Y}, \mathbf{X}_{\parallel}}$ to $\eta_{\mathbf{X}_{\parallel}}$ as $\mathbf{S}_{\text{reduced}}^{\mathbf{x}_{\parallel}}: \mathbb{R}^d \times \mathbb{R}^{n-r} \rightarrow \mathbb{R}^{n-r}$, $(\mathbf{y}, \mathbf{x}_{\parallel}) \mapsto \mathbf{S}_{\text{reduced}}^{\mathbf{x}_{\parallel}}(\mathbf{y}, \mathbf{x}_{\parallel})$. We stress that we don't need to define a reduced map $\mathbf{S}_{\text{reduced}}^{\mathbf{x}_{\perp}}$ and that $\mathbf{S}_{\text{reduced}}^{\mathbf{x}_{\parallel}}$ does not depend on the rotated state coordinates \mathbf{x}_{\perp} . The reduced constrained analysis map $\widetilde{\mathbf{T}}_{\mathbf{y}^*, \text{reduced}}^{\parallel}: \mathbb{R}^d \times \mathbb{R}^{n-r} \rightarrow \mathbb{R}^{n-r}$ reads*

$$\widetilde{\mathbf{T}}_{\mathbf{y}^*, \text{reduced}}^{\parallel}(\mathbf{y}, \mathbf{x}_{\parallel}) = \mathbf{S}_{\text{reduced}}^{\mathbf{x}_{\parallel}}(\mathbf{y}^*, \cdot)^{-1} \circ \mathbf{S}_{\text{reduced}}^{\mathbf{x}_{\parallel}}(\mathbf{y}, \mathbf{x}_{\parallel}). \quad (22)$$

Finally, the reduced constrained analysis map $\widetilde{\mathbf{T}}_{\mathbf{y}^*, \text{reduced}}: \mathbb{R}^d \times \mathbb{R}^n \rightarrow \mathbb{R}^n$ formulated in the original space reads

$$\widetilde{\mathbf{T}}_{\mathbf{y}^*, \text{reduced}}(\mathbf{y}, \mathbf{x}) = \mathbf{U}_{\perp} \mathbf{C} + \mathbf{U}_{\parallel} \widetilde{\mathbf{T}}_{\mathbf{y}^*, \text{reduced}}^{\parallel}(\mathbf{y}, \mathbf{U}_{\parallel}^{\top} \mathbf{x}). \quad (23)$$

Thus, the state update is confined to the affine space $\{\mathbf{x} \in \mathbb{R}^n | \mathbf{U}_{\perp}^{\top} \mathbf{x} = \mathbf{C}\}$, as we only update the state coordinates $\mathbf{U}_{\parallel}^{\top} \mathbf{x}$ spanning this subspace.

6 Specialization to the Gaussian case

In this section, we specialize the constrained analysis map $\widetilde{\mathbf{T}}_{\mathbf{y}^*}$ of (21) for the Gaussian case. Let (\mathbf{Y}, \mathbf{X}) be a pair of random variables with $\mathbf{Y} \in \mathbb{R}^d$ and $\mathbf{X} \in \mathbb{R}^n$ that are jointly Gaussian, i.e.,

$$\begin{bmatrix} \mathbf{Y} \\ \mathbf{X} \end{bmatrix} \sim \mathcal{N} \left(\begin{bmatrix} \boldsymbol{\mu}_{\mathbf{X}} \\ \boldsymbol{\mu}_{\mathbf{Y}} \end{bmatrix}, \begin{bmatrix} \boldsymbol{\Sigma}_{\mathbf{Y}} & \boldsymbol{\Sigma}_{\mathbf{X}, \mathbf{Y}}^{\top} \\ \boldsymbol{\Sigma}_{\mathbf{X}, \mathbf{Y}} & \boldsymbol{\Sigma}_{\mathbf{X}} \end{bmatrix} \right). \quad (24)$$

We define the change of coordinates $\widetilde{\mathbf{U}}$ transforming $(\mathbf{Y}, \mathbf{X}_{\perp}, \mathbf{X}_{\parallel})$ as

$$\widetilde{\mathbf{U}}^{\top} = \begin{bmatrix} \mathbf{I}_d & \mathbf{0}_{d \times n} \\ \mathbf{0}_{d \times n} & \mathbf{U}^{\top} \end{bmatrix} = \begin{bmatrix} \mathbf{I}_d & \mathbf{0}_{d \times n} \\ \mathbf{0}_{d \times r} & \mathbf{U}_{\perp}^{\top} \\ \mathbf{0}_{d \times n-r} & \mathbf{U}_{\parallel}^{\top} \end{bmatrix}. \quad (25)$$

By closure of Gaussian distributions under linear transformations, the distribution for $(\mathbf{Y}, \mathbf{X}_\perp, \mathbf{X}_\parallel)$ is also Gaussian with statistics

$$\begin{bmatrix} \mathbf{Y} \\ \mathbf{X}_\perp \\ \mathbf{X}_\parallel \end{bmatrix} = \tilde{U}^\top \begin{bmatrix} \mathbf{Y} \\ \mathbf{X} \end{bmatrix} \sim \mathcal{N} \left(\begin{bmatrix} \boldsymbol{\mu}_\mathbf{Y} \\ \boldsymbol{\mu}_{\mathbf{X}_\perp} \\ \boldsymbol{\mu}_{\mathbf{X}_\parallel} \end{bmatrix}, \begin{bmatrix} \boldsymbol{\Sigma}_\mathbf{Y} & \boldsymbol{\Sigma}_{\mathbf{X}_\perp, \mathbf{Y}}^\top & \boldsymbol{\Sigma}_{\mathbf{X}_\parallel, \mathbf{Y}}^\top \\ \boldsymbol{\Sigma}_{\mathbf{X}_\perp, \mathbf{Y}} & \boldsymbol{\Sigma}_{\mathbf{X}_\perp} & \boldsymbol{\Sigma}_{\mathbf{X}_\perp, \mathbf{X}_\parallel}^\top \\ \boldsymbol{\Sigma}_{\mathbf{X}_\parallel, \mathbf{Y}} & \boldsymbol{\Sigma}_{\mathbf{X}_\perp, \mathbf{X}_\parallel} & \boldsymbol{\Sigma}_{\mathbf{X}_\parallel} \end{bmatrix} \right). \quad (26)$$

For a generic m -dimensional Gaussian random variable $\mathbf{Z} \sim \mathcal{N}(\boldsymbol{\mu}_\mathbf{Z}, \boldsymbol{\Sigma}_\mathbf{Z})$, we denote by $\mathbf{L}_\mathbf{Z} \in \mathbb{R}^{m \times m}$ the lower Cholesky factor of its inverse covariance matrix, i.e., $\boldsymbol{\Sigma}_\mathbf{Z}^{-1} = \mathbf{L}_\mathbf{Z}^\top \mathbf{L}_\mathbf{Z}$. To construct the Knothe-Rosenblatt rearrangement \mathcal{S} that pushes forward $\pi_{\mathbf{Y}, \mathbf{X}_\perp, \mathbf{X}_\parallel}$ to the standard Gaussian distribution, we introduce the Cholesky factor $\mathbf{L}_\mathbf{Y} \in \mathbb{R}^{d \times d}$, $\mathbf{L}_{\mathbf{X}_\perp | \mathbf{Y}} \in \mathbb{R}^{r \times r}$, $\mathbf{L}_{\mathbf{X}_\parallel | \mathbf{Y}, \mathbf{X}_\perp} \in \mathbb{R}^{(n-r) \times (n-r)}$ of the inverse covariance matrix $\boldsymbol{\Sigma}_\mathbf{Y}^{-1}$, $\boldsymbol{\Sigma}_{\mathbf{X}_\perp | \mathbf{Y}}^{-1}$, $\boldsymbol{\Sigma}_{\mathbf{X}_\parallel | \mathbf{Y}, \mathbf{X}_\perp}^{-1}$, respectively. These are explicitly given by

$$\begin{aligned} \boldsymbol{\Sigma}_\mathbf{Y}^{-1} &= \mathbf{L}_\mathbf{Y}^\top \mathbf{L}_\mathbf{Y} \\ \boldsymbol{\Sigma}_{\mathbf{X}_\perp | \mathbf{Y}}^{-1} &= \mathbf{L}_{\mathbf{X}_\perp | \mathbf{Y}}^\top \mathbf{L}_{\mathbf{X}_\perp | \mathbf{Y}} \\ \boldsymbol{\Sigma}_{\mathbf{X}_\parallel | \mathbf{Y}, \mathbf{X}_\perp}^{-1} &= \mathbf{L}_{\mathbf{X}_\parallel | \mathbf{Y}, \mathbf{X}_\perp}^\top \mathbf{L}_{\mathbf{X}_\parallel | \mathbf{Y}, \mathbf{X}_\perp}. \end{aligned} \quad (27)$$

Using classical results on the conditional mean of Gaussian random variables, we obtain the Knothe-Rosenblatt rearrangement \mathcal{S} that pushes forward $\pi_{\mathbf{Y}, \mathbf{X}_\perp, \mathbf{X}_\parallel}$ to $\eta_\mathbf{Y} \otimes \eta_{\mathbf{X}_\perp} \otimes \eta_{\mathbf{X}_\parallel}$, see [Spantini et al., 2022, Le Provost et al., 2023] as

$$\mathcal{S}(\mathbf{y}, \mathbf{x}_\perp, \mathbf{x}_\parallel) = \begin{bmatrix} \mathcal{S}^\mathbf{Y}(\mathbf{y}) \\ \mathcal{S}^{\mathbf{X}_\perp}(\mathbf{y}, \mathbf{x}_\perp) \\ \mathcal{S}^{\mathbf{X}_\parallel}(\mathbf{y}, \mathbf{x}_\perp, \mathbf{x}_\parallel) \end{bmatrix} = \begin{bmatrix} \mathbf{L}_\mathbf{Y}(\mathbf{y} - \boldsymbol{\mu}_\mathbf{Y}) \\ \mathbf{L}_{\mathbf{X}_\perp | \mathbf{Y}}(\mathbf{x}_\perp - \boldsymbol{\mu}_{\mathbf{X}_\perp | \mathbf{Y}}) \\ \mathbf{L}_{\mathbf{X}_\parallel | \mathbf{Y}, \mathbf{X}_\perp}(\mathbf{x}_\parallel - \boldsymbol{\mu}_{\mathbf{X}_\parallel | \mathbf{Y}, \mathbf{X}_\perp}) \end{bmatrix}. \quad (28)$$

By specializing the formulas (16) and (18) to the triangular map $\mathcal{S}(\mathbf{y}, \mathbf{x}_\perp, \mathbf{x}_\parallel)$ of (28), we obtain

$$\begin{aligned} \mathbf{T}_{\mathbf{y}^*}^\perp(\mathbf{y}, \mathbf{x}_\perp) &= \mathbf{x}_\perp - \boldsymbol{\Sigma}_{\mathbf{X}_\perp, \mathbf{Y}} \boldsymbol{\Sigma}_\mathbf{Y}^{-1}(\mathbf{y} - \mathbf{y}^*), \\ \mathbf{T}_{\mathbf{y}^*}^\parallel(\mathbf{y}, \mathbf{x}_\perp, \mathbf{x}_\parallel) &= \mathbf{x}_\parallel - \boldsymbol{\Sigma}_{\mathbf{X}_\parallel, \mathbf{Y}} \boldsymbol{\Sigma}_\mathbf{Y}^{-1}(\mathbf{y} - \mathbf{y}^*). \end{aligned} \quad (29)$$

Note that the formula for $\mathbf{T}_{\mathbf{y}^*}^\perp$ and $\mathbf{T}_{\mathbf{y}^*}^\parallel$ corresponds to the Kalman filter update in the subspace spanned by the columns of \mathbf{U}_\perp and \mathbf{U}_\parallel , respectively. Remarkably, despite the recursive update of the state components (first updating \mathbf{x}_\perp then \mathbf{x}_\parallel) in the generic nonlinear case, the analysis map $\mathbf{T}_{\mathbf{y}^*}^\parallel(\mathbf{y}, \mathbf{x}_\perp, \mathbf{x}_\parallel)$ in the Gaussian case does not depend on \mathbf{x}_\perp . This suggests that we can fully decouple the update of the different state components with the Kalman filter, echoing a similar conclusion in the context of Kalman smoothers by Ramgraber et al. [2023]. The analysis map in the original space $\mathbf{T}_{\mathbf{y}^*}$ now reads

$$\begin{aligned} \mathbf{T}_{\mathbf{y}^*}(\mathbf{y}, \mathbf{x}) &= \mathbf{U}_\perp \mathbf{T}_{\mathbf{y}^*}^\perp(\mathbf{y}, \mathbf{x}_\perp) + \mathbf{U}_\parallel \mathbf{T}_{\mathbf{y}^*}^\parallel(\mathbf{y}, \mathbf{x}_\perp, \mathbf{x}_\parallel) \\ &= \mathbf{U}_\perp (\mathbf{x}_\perp - \boldsymbol{\Sigma}_{\mathbf{X}_\perp, \mathbf{Y}} \boldsymbol{\Sigma}_\mathbf{Y}^{-1}(\mathbf{y} - \mathbf{y}^*)) + \mathbf{U}_\parallel (\mathbf{x}_\parallel - \boldsymbol{\Sigma}_{\mathbf{X}_\parallel, \mathbf{Y}} \boldsymbol{\Sigma}_\mathbf{Y}^{-1}(\mathbf{y} - \mathbf{y}^*)) \\ &= \mathbf{U}_\perp (\mathbf{U}_\perp^\top \mathbf{x}) + \mathbf{U}_\parallel (\mathbf{U}_\parallel^\top \mathbf{x}) - \mathbf{U}_\perp \mathbf{U}_\perp^\top \boldsymbol{\Sigma}_{\mathbf{X}_\perp, \mathbf{Y}} \boldsymbol{\Sigma}_\mathbf{Y}^{-1}(\mathbf{y} - \mathbf{y}^*) - \mathbf{U}_\parallel \mathbf{U}_\parallel^\top \boldsymbol{\Sigma}_{\mathbf{X}_\parallel, \mathbf{Y}} \boldsymbol{\Sigma}_\mathbf{Y}^{-1}(\mathbf{y} - \mathbf{y}^*) \\ &= \mathbf{x} - \boldsymbol{\Sigma}_{\mathbf{X}, \mathbf{Y}} \boldsymbol{\Sigma}_\mathbf{Y}^{-1}(\mathbf{y} - \mathbf{y}^*), \end{aligned} \quad (30)$$

where the last two equations rely on $\mathbf{x}_\perp = \mathbf{U}_\perp^\top \mathbf{x}$ and $\mathbf{U} = [\mathbf{U}_\perp, \mathbf{U}_\parallel]$ being orthonormal. As noted in the previous section, rotating the state components, performing the inference in these new coordinates, and lifting the result to the original space is strictly equivalent to performing the inference in the original space. Thus, it is natural that the analysis map of (19) in the Gaussian case reverts to the Kalman filter update. Similarly, we obtain the (constrained) analysis

map $\tilde{T}_{\mathbf{y}^*}$ preserving the invariant $\mathbf{H}(\mathbf{x}) = \mathbf{U}_\perp^\top \mathbf{x}$ as

$$\begin{aligned} \tilde{T}_{\mathbf{y}^*}(\mathbf{y}, \mathbf{x}) &= \mathbf{U}_\perp \mathbf{x}_\perp + \mathbf{U}_\parallel T_{\mathbf{y}^*}^\parallel(\mathbf{y}, \mathbf{x}_\perp, \mathbf{x}_\parallel) \\ &= \mathbf{x} - \mathbf{U}_\parallel \mathbf{U}_\parallel^\top \Sigma_{\mathbf{X}, \mathbf{Y}} \Sigma_{\mathbf{Y}}^{-1} (\mathbf{y} - \mathbf{y}^*) \\ &= \mathbf{x} - (\mathbf{I} - \mathbf{U}_\perp \mathbf{U}_\perp^\top) \Sigma_{\mathbf{X}, \mathbf{Y}} \Sigma_{\mathbf{Y}}^{-1} (\mathbf{y} - \mathbf{y}^*). \end{aligned} \tag{31}$$

We conclude this section with several comments on this last result. First, the constrained analysis map corresponds to a Kalman-like update where the Kalman gain is projected on the orthonormal complement of \mathbf{U}_\perp , namely on the space spanned by the columns of \mathbf{U}_\parallel . Interestingly, (31) establishes an equivalence between an “embedding approach” and a “projective approach” [Simon, 2010]. In the first case, we perform a constrained inference in the rotated space before lifting back the result. In the latter case, we “naively” project the state’s update $-\Sigma_{\mathbf{X}, \mathbf{Y}} \Sigma_{\mathbf{Y}}^{-1} (\mathbf{y} - \mathbf{y}^*)$ onto the columns of \mathbf{U}_\parallel to ensure that the invariant is unchanged. While there is no reason for these two approaches to coincide in the non-Gaussian case with arbitrary invariants, (31) states that they are equivalent in the Gaussian case with linear invariants \mathbf{H} . In the case where the linear invariants are constant over the prior —see Remark 7 for the general treatment— we can specialize the reduced transformations of Remark 7 to derive a reduced constrained analysis map $\tilde{T}_{\mathbf{y}^*, \text{reduced}}$ of (23) in the Gaussian case. We show that the resulting map is identical to the fully supported case, since the unconstrained map $T_{\mathbf{y}^*}^\parallel(\mathbf{y}, \mathbf{x}_\perp, \mathbf{x}_\parallel)$ of (29) does not depend on \mathbf{x}_\perp . We omit details for brevity.

7 Preserving linear invariants with Kalman filters

It is often claimed that the **vanilla** Kalman filter and its Monte Carlo approximation, namely the ensemble Kalman filter, preserve linear invariants. This section addresses this claim—and its important nuances—in two particular scenarios. In the first scenario, we assume that the linear invariants are constant over the prior distribution $\pi_{\mathbf{X}}$, i.e., $\mathbf{H}(\mathbf{x}) = \mathbf{C} \in \mathbb{R}^r$ for any realization \mathbf{x} of \mathbf{X} . In the second scenario, we assume that the expected linear invariants of the prior distribution are known, i.e., $\mathbb{E}_{\pi_{\mathbf{X}}}[\mathbf{H}(\mathbf{x})] = \mathbf{C} \in \mathbb{R}^r$. This can model a scenario where the true invariant is known up to some uncertainty.

Importantly, the empirical Kalman gain often needs to be regularized with covariance tapering or inflation to alleviate undesired sampling effects such as rank deficiency, spurious long-range correlations, and underestimation of the statistics. However, such modifications are known to break the linear preserving properties of the vanilla ensemble Kalman filter [Janjić et al., 2014]. As a result, we will show below that the ensemble Kalman filter only preserves linear invariants when no regularization techniques are applied and when the linear invariants are constant over the prior distribution (the first scenario). In contrast, the constrained Kalman filter and the constrained ensemble Kalman filter, presented in the previous section, intrinsically preserve linear invariants in both of the above scenarios.

7.1 Scenario 1: The linear invariants are constant over the prior distribution

In this first scenario, we assume that the linear invariants are constant over the prior distribution $\pi_{\mathbf{X}}$, i.e., $\mathbf{H}(\mathbf{x}) = \mathbf{C} \in \mathbb{R}^r$ for any realization \mathbf{x} of \mathbf{X} . Then it is clear that $\mathbb{E}_{\pi_{\mathbf{X}}}[\mathbf{H}(\mathbf{x})] = \mathbf{C}$. Recalling that the analysis map of the Kalman filter T_{KF} is given in (30) as $T_{\text{KF}}(\mathbf{y}, \mathbf{x}) = \mathbf{x} - \Sigma_{\mathbf{X}, \mathbf{Y}} \Sigma_{\mathbf{Y}}^{-1} (\mathbf{y} - \mathbf{y}^*)$, where $\Sigma_{\mathbf{X}, \mathbf{Y}}$ denotes the cross-covariance between the

state \mathbf{X} and the observation \mathbf{Y} , we get for $(\mathbf{y}, \mathbf{x}) \in \mathbb{R}^d \times \mathbb{R}^n$

$$\begin{aligned}
 \mathbf{H}(\mathbf{T}_{\text{KF}}(\mathbf{y}, \mathbf{x})) &= \mathbf{U}_{\perp}^{\top} \mathbf{T}_{\text{KF}}(\mathbf{y}, \mathbf{x}), \\
 &= \mathbf{U}_{\perp}^{\top} \mathbf{x} - \mathbf{U}_{\perp}^{\top} \Sigma_{\mathbf{X}, \mathbf{Y}} \Sigma_{\mathbf{Y}}^{-1} (\mathbf{y} - \mathbf{y}^*), \\
 &= \mathbf{U}_{\perp}^{\top} \mathbf{x} - \mathbf{U}_{\perp}^{\top} \left[\int (\mathbf{x}' - \boldsymbol{\mu}_{\mathbf{X}}) (\mathbf{y}' - \boldsymbol{\mu}_{\mathbf{Y}})^{\top} d\pi_{\mathbf{Y}, \mathbf{X}}(\mathbf{y}', \mathbf{x}') \right] \Sigma_{\mathbf{Y}}^{-1} (\mathbf{y} - \mathbf{y}^*), \\
 &= \mathbf{U}_{\perp}^{\top} \mathbf{x} - \left[\int \mathbf{U}_{\perp}^{\top} (\mathbf{x}' - \boldsymbol{\mu}_{\mathbf{X}}) \pi_{\mathbf{X}}(\mathbf{x}') \left[\int \pi_{\mathbf{Y} | \mathbf{X}}(\mathbf{y}' | \mathbf{x}') (\mathbf{y}' - \boldsymbol{\mu}_{\mathbf{Y}})^{\top} d\mathbf{y}' \right] d\mathbf{x}' \right] \Sigma_{\mathbf{Y}}^{-1} (\mathbf{y} - \mathbf{y}^*), \\
 &= \mathbf{U}_{\perp}^{\top} \mathbf{x} - \left[\int \left(\mathbf{U}_{\perp}^{\top} \mathbf{x}' \pi_{\mathbf{X}}(\mathbf{x}') - \mathbf{U}_{\perp}^{\top} \boldsymbol{\mu}_{\mathbf{X}} \pi_{\mathbf{X}}(\mathbf{x}') \right) \left[\int \pi_{\mathbf{Y} | \mathbf{X}}(\mathbf{y}' | \mathbf{x}') (\mathbf{y}' - \boldsymbol{\mu}_{\mathbf{Y}})^{\top} d\mathbf{y}' \right] d\mathbf{x}' \right] \Sigma_{\mathbf{Y}}^{-1} (\mathbf{y} - \mathbf{y}^*), \\
 &= \mathbf{U}_{\perp}^{\top} \mathbf{x} - \left[\int \mathbf{C} \pi_{\mathbf{X}}(\mathbf{x}') - \mathbf{C} \pi_{\mathbf{X}}(\mathbf{x}') \left[\int \pi_{\mathbf{Y} | \mathbf{X}}(\mathbf{y}' | \mathbf{x}') (\mathbf{y}' - \boldsymbol{\mu}_{\mathbf{Y}})^{\top} d\mathbf{y}' \right] d\mathbf{x}' \right] \Sigma_{\mathbf{Y}}^{-1} (\mathbf{y} - \mathbf{y}^*), \\
 &= \mathbf{U}_{\perp}^{\top} \mathbf{x} - \mathbf{0}_r, \\
 &= \mathbf{H}(\mathbf{x}),
 \end{aligned} \tag{32}$$

where we use that for $\mathbf{x}' \in \mathbb{R}^n$ that is not in the support of $\pi_{\mathbf{X}}$, i.e., $\pi_{\mathbf{X}}(\mathbf{x}') = 0$, we have $\mathbf{U}_{\perp}^{\top} \mathbf{x}' \pi_{\mathbf{X}}(\mathbf{x}') = \mathbf{U}_{\perp}^{\top} \mathbf{x}' \pi_{\mathbf{X}}(\mathbf{x}') = \mathbf{U}_{\perp}^{\top} \mathbf{x}' \times 0 = \mathbf{C} \pi_{\mathbf{X}}(\mathbf{x}')$. Hence, in this scenario, we have $\mathbf{U}_{\perp}^{\top} \mathbf{x}' \pi_{\mathbf{X}}(\mathbf{x}') = \mathbf{C} \pi_{\mathbf{X}}(\mathbf{x}')$ for any $\mathbf{x}' \in \mathbb{R}^n$. Thus, the invariant is preserved by \mathbf{T}_{KF} if it is constant over $\pi_{\mathbf{X}}$. We note that a similar derivation holds for the analysis map of the ensemble Kalman filter, where the covariance matrices $\Sigma_{\mathbf{X}, \mathbf{Y}}$ and $\Sigma_{\mathbf{Y}}$ are replaced by their empirical counterparts estimated from samples $\{(\mathbf{y}^{(i)}, \mathbf{x}^{(i)})\}$ of the joint distribution of the observations and states. Finally, we stress that this result holds for any joint distribution $\pi_{\mathbf{Y}, \mathbf{X}}$ with finite second-order moments, i.e., $\Sigma_{\mathbf{Y}, \mathbf{X}}$ and $\Sigma_{\mathbf{Y}}$ are finite.

7.2 Scenario 2: The expected value of the linear invariants over the prior is known

In this second scenario, we assume that the expected linear invariants of the prior distribution are known, i.e., $\mathbb{E}_{\pi_{\mathbf{X}}} [\mathbf{H}(\mathbf{x})] = \mathbf{C} \in \mathbb{R}^r$ is known. We investigate whether the Kalman filter preserves the expected linear invariants by checking if $\mathbb{E}_{\pi_{\mathbf{Y}, \mathbf{X}}} [\mathbf{H}(\mathbf{T}_{\text{KF}}(\mathbf{y}, \mathbf{x}))] = \mathbf{C}$ is satisfied. To this end, note that (30) implies

$$\begin{aligned}
 \mathbb{E}_{\pi_{\mathbf{Y}, \mathbf{X}}} [\mathbf{H}(\mathbf{T}_{\text{KF}}(\mathbf{y}, \mathbf{x}))] &= \mathbb{E}_{\pi_{\mathbf{Y}, \mathbf{X}}} \left[\mathbf{U}_{\perp}^{\top} \mathbf{x} \right] - \mathbb{E}_{\pi_{\mathbf{Y}, \mathbf{X}}} \left[\mathbf{U}_{\perp}^{\top} \Sigma_{\mathbf{X}, \mathbf{Y}} \Sigma_{\mathbf{Y}}^{-1} (\mathbf{y} - \mathbf{y}^*) \right] \\
 &= \mathbf{C} - \mathbf{U}_{\perp}^{\top} \Sigma_{\mathbf{X}, \mathbf{Y}} \Sigma_{\mathbf{Y}}^{-1} (\boldsymbol{\mu}_{\mathbf{Y}} - \mathbf{y}^*).
 \end{aligned} \tag{33}$$

Thus, the Kalman filter does not necessarily preserve the expected linear invariants of the prior $\pi_{\mathbf{X}}$. To be more precise, (33) implies that the Kalman filter preserves the expected linear invariants of the prior $\pi_{\mathbf{X}}$ if and only if $\mathbf{U}_{\perp}^{\top} \mathbf{b} = \mathbf{0}_r$ with “expected state update” $\mathbf{b} = \Sigma_{\mathbf{X}, \mathbf{Y}} \Sigma_{\mathbf{Y}}^{-1} (\boldsymbol{\mu}_{\mathbf{Y}} - \mathbf{y}^*) \in \mathbb{R}^n$. We can interpret this as \mathbf{b} lying in the span of the columns of \mathbf{U}_{\parallel} and, therefore, not containing any information about the linear invariants.

To summarize our exploration of these two scenarios: The regularized EnKF generally does not preserve linear invariants of the prior distribution. In contrast, the constrained Kalman filter (31) preserves the linear invariants of any realization of the prior distribution $\pi_{\mathbf{X}}$. In other words, the distribution $\pi_{\mathbf{H}(\mathbf{X})}$ is unchanged by the constrained analysis map $\tilde{\mathbf{T}}_{\mathbf{y}^*}$.

8 Computational examples

This section presents the results of our numerical examples on preserving linear invariants with ensemble Kalman filters and stochastic map filters. We consider three examples: a synthetic linear ordinary differential equation (ODE) with an arbitrary number of linear invariants, the linear advection equation as the (arguably simplest) prototype of a hyperbolic conservation law, and an embedding of the nonlinear Lorenz-63 model in \mathbb{R}^4 with a linear invariant.

For reproducibility, the code of our numerical experiments is available at <https://github.com/mleprovost/Paper-Linear-Invariants-Ensemble-Filters>.

8.1 Numerical setup

This section discusses common considerations in our data assimilation experiments. To isolate the performance of the filtering algorithms, we perform a “twin experiment” where the same state-space model is used to generate the ground truth and in the forecast and analysis steps of the ensemble filters [Asch et al., 2016]. The ground truth is generated by sampling an initial state \mathbf{x}_0^* from the initial distribution $\pi_{\mathbf{x}_0}$ and evolving it through the dynamical model (1) over the time interval $[0, t_f]$. Discretizing $[0, t_f]$ using an equidistant grid with step size Δt_{obs} , at each time step, we collect the true state \mathbf{x}_t^* and generate a noisy observation \mathbf{y}_t^* from the observation model (2). Although we might not know the transition kernel $\pi_{\mathbf{x}_t | \mathbf{x}_{t-1}}$ and the likelihood model $\pi_{\mathbf{y}_t | \mathbf{x}_{t-1}}$, we assume that we can generate samples from them. Furthermore, we assume that the observation operator \mathbf{g} is linear and given by $\mathbf{g}(\mathbf{x}_t) = \mathbf{G}\mathbf{x}_t$ with observation matrix $\mathbf{G} \in \mathbb{R}^{d \times n}$. In the filtering setting that underpins this work, we seek to estimate the true state $\{\mathbf{x}_t^*\}$ in a sequential way given the noisy observations $\{\mathbf{y}_t^*\}$ of the true process and the initial distribution $\pi_{\mathbf{x}_0}$.

To ensure that the process noise \mathbf{W}_t in the dynamical model (1) does not change the linear invariants $\mathbf{H}(\mathbf{x}) = \mathbf{U}_\perp^\top \mathbf{x}$, we consider a linear invariant-preserving Gaussian process noise with zero mean and covariance $\sigma_{\mathbf{W}_t}^2 \mathbf{I}_n$ with $\sigma_{\mathbf{W}_t} > 0$. To sample from this distribution, we project the noise samples from $\mathcal{N}(\mathbf{0}_n, \sigma_{\mathbf{W}_t}^2 \mathbf{I}_n)$ on the columns of \mathbf{U}_\parallel spanning the (orthogonal) complement of $\text{span}(\mathbf{U}_\perp)$. We stress that the numerical schemes used in this work preserve the linear invariants of the dynamical systems. Thus, violations of these invariants can be fully attributed to flaws in the filtering algorithms.

Our first two experiments consist of linear Gaussian filtering problems, for which we compare two related ensemble filters: the stochastic ensemble Kalman filter [Evensen, 1994] without constraints on the linear invariants, called unconstrained EnKF (UnEnKF), and the proposed stochastic ensemble Kalman filter that preserves linear invariants by building a Monte Carlo approximation of the analysis map (31), called constrained EnKF (ConsEnKF). For both filters, we apply multiplicative inflation and covariance tapering to regularize the empirical estimate of the Kalman gain, see [Asch et al., 2016] for more details. We stress that these techniques are critical for successful state estimation with ensemble Kalman filters with limited samples but are also known to break linear invariants [Janjić et al., 2014]. The constrained EnKF combines the previous regularization techniques with a projection on the span of \mathbf{U}_\parallel to preserve linear invariants. Algorithm 2 in Appendix E provides a pseudo-code for the constrained EnKF.

For the first two linear-Gaussian filtering experiments, the filtering distribution is Gaussian. Thus, nonlinear filters such as the stochastic map filter, offer no advantage over the ensemble Kalman filter. In the third experiment, we consider a non-Gaussian filtering problem with a linear invariant, for which we compare unconstrained/constrained stochastic map

filters with the EnKF. We provide an overview of the parameterization of the stochastic map filter in Appendix C, but refer readers to [Spantini et al., 2022] for further details. Algorithm 1 in Appendix D provides a pseudo-code for the constrained SMF.

We assess the performance of the different ensemble filters with the root-mean-square-error (RMSE) and the spread of the posterior ensemble. Recall that the RMSE at time t is defined as $\text{RMSE}_t = \|\mathbf{x}_t^* - \hat{\boldsymbol{\mu}}_{t,a}\|_2 / \sqrt{n}$, where $\hat{\boldsymbol{\mu}}_{t,a} \in \mathbb{R}^n$ is the filtering ensemble mean at time t , and n is the dimension of the state variable. The spread at time t is given by $\text{spread}_t = \text{tr}(\hat{\boldsymbol{\Sigma}}_{t,a}) / \sqrt{n}$, where $\hat{\boldsymbol{\Sigma}}_{t,a} \in \mathbb{R}^{n \times n}$ is the filtering ensemble covariance at time t . The filters are run over 2000 assimilation cycles, and we discard the first 1000 assimilation cycles so that the statistics are approximately stationary. After this spin-up phase, we report the time-averaged metrics of the ensemble filters with optimally tuned multiplicative inflation and/or covariance tapering, achieving the lowest RMSE for a given ensemble size.

8.2 A synthetic linear model with arbitrary number of linear invariants

In this first example, we consider a synthetic linear ODE model for which we can fix an arbitrary number of linear invariants. This allows us to investigate the performance of the proposed ConsEnKF, compared to the existing UnEnKF, for different numbers of invariants r and ensemble sizes M .

Consider the linear dynamical model

$$\begin{aligned} \frac{d\mathbf{x}}{dt} &= \mathbf{A}_r \mathbf{x}, \\ \mathbf{x}(0) &= \mathbf{x}_0, \end{aligned} \tag{34}$$

where $\mathbf{x}_0 \in \mathbb{R}^n$ and the matrix $\mathbf{A}_r \in \mathbb{R}^{n \times n}$ is semi-negative definite, i.e., symmetric with non-positive eigenvalues, with spectral decomposition

$$\mathbf{A}_r = \mathbf{U} \mathbf{D}_{\Lambda_r} \mathbf{U}^{-1}, \tag{35}$$

where $\mathbf{U} \in \mathbb{R}^{n \times n}$ is an orthonormal matrix and $\mathbf{D}_{\Lambda_r} \in \mathbb{R}^{n \times n}$ denotes the diagonal matrix with diagonal entries $\Lambda_r \in \mathbb{R}^n$. The dynamic model (34) is motivated by production-destruction systems in atmospheric chemistry for which preserving linear invariants has been demonstrated to be crucial for accurate and robust numerical simulations [Nüßlein et al., 2021, Huang et al., 2022, Izgin et al., 2023, Izgin and Öffner, 2023].

Without loss of generality, we assume that the vector of eigenvalues Λ_r is organized as follows:

$$\Lambda_r = [\mathbf{0}_r, -\lambda_{r+1}, \dots, -\lambda_n], \text{ with } \lambda_k > 0 \text{ for } k > r. \tag{36}$$

We use the underscore r to stress that 0 is an eigenvalue of \mathbf{A}_r with multiplicity r . We choose nonnegative eigenvalues for \mathbf{A}_r to produce a linear dynamical model (34) with stable solutions [Huang et al., 2022]. From classical results on time-invariant linear systems, the solution $\mathbf{x}(t)$ of (34) is given by

$$\mathbf{x}(t) = \exp(\mathbf{A}_r t) \mathbf{x}_0. \tag{37}$$

Using the eigendecomposition of \mathbf{A}_r , we get $\mathbf{x}(t) = \mathbf{U} \exp(\mathbf{D}_{\Lambda_r} t) \mathbf{U}^T \mathbf{x}_0$. We denote by $\mathbf{U}_\perp \in \mathbb{R}^{n \times r}$ the first r orthonormal columns of \mathbf{U} and by \mathbf{U}_\parallel the remaining $(n - r)$ orthonormal columns. Thus, we can verify that the linear

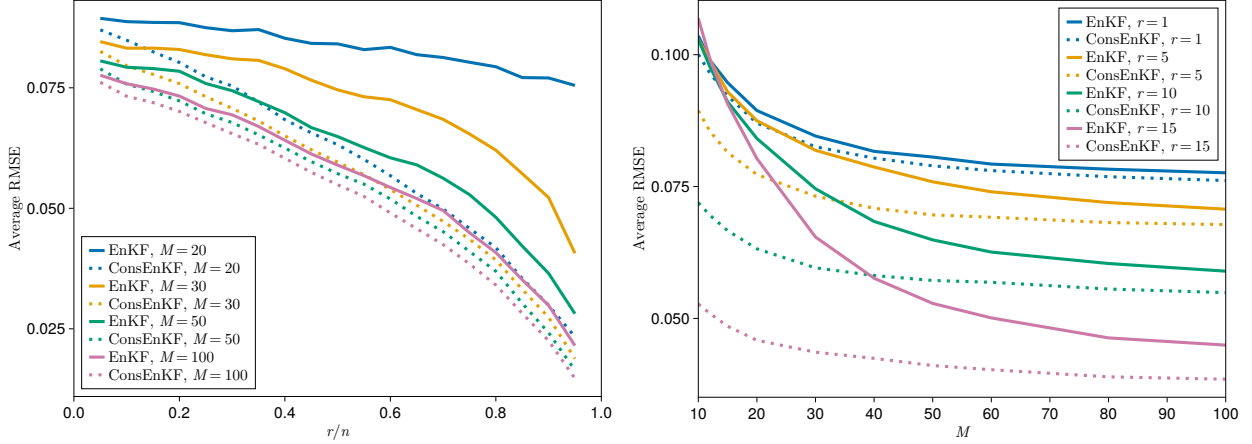


Figure 2: Left panel: Evolution of the time-averaged RMSE for the unconstrained EnKF (solid lines) and the constrained EnKF (dashed lines) for varying ratios $r/n \in [0, 1]$ between the number of linear invariants r and the problem dimension n with $M = 20, 30, 50, 100$ samples. Right panel: Evolution of the time-averaged RMSE for the unconstrained EnKF (solid lines) and the constrained EnKF (dashed lines) for varying ensemble sizes M with $r = 1, 5, 10, 15$. Both filters use optimally tuned multiplicative inflation and covariance tapering.

invariants $U_{\perp}^{\top} \mathbf{x}_0 = \mathbf{C}_0 \in \mathbb{R}^r$ are preserved by (34):

$$\begin{aligned}
 U_{\perp}^{\top} \mathbf{x}(t) &= U_{\perp}^{\top} U \exp(\mathbf{D}_{\Lambda_r} t) U^{\top} \mathbf{x}_0, \\
 &= U_{\perp}^{\top} U_{\perp} \mathbf{D}_{\mathbf{1}_r} U_{\perp}^{\top} \mathbf{x}_0 + U_{\perp}^{\top} U_{\parallel} \mathbf{D}_{[\exp(-\lambda_{r+1} t), \dots, \exp(-\lambda_n t)]} U_{\parallel}^{\top} \mathbf{x}_0, \\
 &= \mathbf{I}_r \mathbf{C}_0 + \mathbf{0}_r, \\
 &= \mathbf{C}_0,
 \end{aligned} \tag{38}$$

where we have used that $U_{\perp}^{\top} U_{\perp} = \mathbf{I}_r$, $U_{\perp}^{\top} U_{\parallel} = \mathbf{0}_{r \times (n-r)}$, and $\exp(\mathbf{D}_{\Lambda_r} t) = \mathbf{D}_{[\mathbf{1}_r, \exp(-\lambda_{r+1} t), \dots, \exp(-\lambda_n t)]}$. We denote by $\mathbf{1}_r \in \mathbb{R}^r$ the vector of ones of length r .

From the continuous dynamical model (34), we construct a discrete time forward operator \mathbf{f} for the dynamical model (1) by integration of (34) over a time step Δt_{obs} between two assimilation cycles, i.e., $\mathbf{f}(\mathbf{x}_t) = \exp(\mathbf{A}_r \Delta t_{\text{obs}}) \mathbf{x}_t$. As mentioned above, this setting allows a parametric study of the performance metrics over the ratio of linear invariants $r/n \in [0, 1]$ (with state dimension n) and the ensemble size M .

We consider a state of dimension $n = 20$. The eigenvalues $-\lambda_k$ for $k > r$ are independently drawn from a uniform distribution on $[-5, 0]$. The time step size between two assimilation cycles is $\Delta t_{\text{obs}} = 10^{-1}$. We use a Gaussian linear invariant-preserving process noise with zero mean and covariance $\sigma_{\mathbf{w}_t}^2 \mathbf{I}_n$ with $\sigma_{\mathbf{w}_t} = 10^{-2}$. We observe every component of the state, i.e., $d = n = 20$, corrupted by an additive Gaussian observation noise with zero mean and covariance $\sigma_{\mathcal{E}}^2 \mathbf{I}_d$ with $\sigma_{\mathcal{E}} = 10^{-1}$.

Figure 2 compares the RMSE of the unconstrained EnKF and the constrained EnKF for different ensemble sizes M and ratios r/n between the number of linear invariants r and the problem dimension n . Preserving the linear invariants consistently results in a reduction of the RMSE. For $r/n < 0.1$, the improvements are at around 5%, showing little variation with the ensemble size M . As r/n increases, we observe larger RMSE improvement for all ensemble sizes

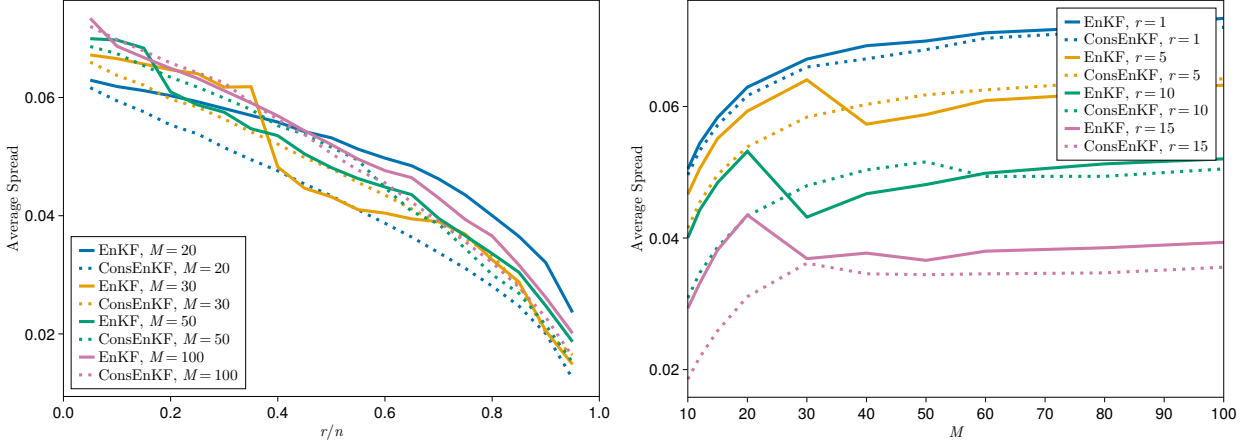


Figure 3: Left panel: Evolution of the time-averaged spread for the unconstrained EnKF (solid lines) and the constrained EnKF (dashed lines) for varying ratios $r/n \in [0, 1]$ with $M = 20, 30, 50, 100$ samples. Right panel: Evolution of the time-averaged spread for the unconstrained EnKF (solid lines) and the constrained EnKF (dashed lines) for varying ensemble sizes M with $r = 1, 5, 10, 15$. Both filters use optimally tuned multiplicative inflation and covariance tapering.

M . Specifically, for $M = 20$ and $r = 19$, the RMSE of the unconstrained EnKF is $7.7 \cdot 10^{-2}$, while the RMSE of the constrained EnKF is $2.5 \cdot 10^{-2}$, corresponding to a reduction of the RMSE by 67%. Moreover, for small ensemble sizes $M < 40$, the RMSE improvements are significant and increase with the number of linear invariants. For $M = 10$ and $r = 10$, the RMSE is reduced by 36%. For a fixed number of invariants r , the RMSE improvement due to preserving linear invariants decreases with the ensemble size M . This is consistent with the empirical Kalman gain estimate requiring less regularization as the ensemble size M increases. Thus, the analysis map of the unconstrained EnKF gets closer to the analysis map of the vanilla EnKF. From Section 7.1, the vanilla EnKF preserves linear invariants if all the forecast samples have the same invariants. We can expect that the violations of the linear invariants of the UnEnKF reduce in magnitude as the ensemble size M increases, thus reducing the benefits of preserving linear invariants as the ensemble size increases.

Figure 2 reports on the spread of the unconstrained EnKF and the constrained EnKF. We do not observe significant differences in the spread of the unconstrained EnKF and the constrained EnKF. We conclude that preserving linear invariants is particularly advantageous for the RMSE when the ensemble size M is small and the ratio of linear invariants r/n is large. We interpret these results as a reduction of the variance of the empirical Kalman gain by constraining the image space of the estimated Kalman gain to the subspace spanned by the columns of U_{\parallel} . We refer readers to [Le Provost et al., 2022] for further discussions on the benefits of linear dimension reductions for the ensemble Kalman filter.

8.3 Linear advection on periodic domain

Consider the one-dimensional linear advection equation for a field $u(s, t)$ on the periodic domain $\Omega = [0, 1)$:

$$\begin{aligned} \frac{\partial u(s, t)}{\partial t} + \nabla \cdot (cu(s, t)) &= 0, & s \in \Omega, t > 0, \\ u(s, 0) &= u_0(s), & s \in \Omega, \end{aligned} \quad (39)$$

where $u_0: \mathbb{R} \rightarrow \mathbb{R}$ is the initial field, $c = 1$ is the advection velocity. Notably, due to the periodic boundary conditions, the total mass $m(t) = \int_{\Omega} u(s, t) ds$ of exact solutions $u(s, t)$ of (39) is constant in time, i.e., $m(t) = m(0)$ for all t , and numerical solutions should mimic this behavior on a discrete level. We discretize the domain $\Omega = [0, 1)$ with $n = 128$ grid nodes $\{s_k\}$. The state vector \mathbf{x}_t at time t is given by the pointwise evaluations of the continuous field at the grid nodes $\{s_j\}$, i.e., $\mathbf{x}_{t,k} = u(s_k, t)$ for $k = 1, \dots, n$. To solve (39), we use a spectral method for the spatial discretization and a fourth-order adaptive strong stability preserving (SSP) Runge–Kutta (RK) time integration scheme (SSPRK43), see [Brunton and Kutz, 2019, Rackauckas and Nie, 2017]. The distribution $\pi_{\mathbf{x}_0}$ used to generate the true initial condition and the initial ensemble member is given by an n -dimensional smooth and periodic distribution, denoted $\mathcal{S}_{n,r}(\mathbf{U}_{\perp}, \mathbf{C}, \alpha)$, that is parameterized by a sub-unitary matrix $\mathbf{U}_{\perp} \in \mathbb{R}^{n \times r}$, a vector $\mathbf{C} \in \mathbb{R}^r$, and a smoothing parameter $\alpha > 0$. By design, a random variable $\mathbf{X} \sim \mathcal{S}_n(\mathbf{U}_{\perp}, \mathbf{C}, \alpha)$ satisfies $\mathbf{U}_{\perp}^{\top} \mathbf{X} = \mathbf{C}$. To generate samples from the distribution $\mathcal{S}_n(\mathbf{U}_{\perp}, \mathbf{C}, \alpha)$, we proceed in three steps:

- (i) Generate samples $z_{\text{Re}}, z_{\text{Im}}$ from the $(n/2 + 1)$ -dimensional standard Gaussian distribution $\mathcal{N}(\mathbf{0}, \mathbf{I})$;
- (ii) Compute $\tilde{\mathbf{x}} \in \mathbb{C}^{\frac{n}{2}+1}$ with components $\tilde{x}_k = (z_{\text{Re},k} + i z_{\text{Im},k}) \exp(-\frac{1}{2}k^{\alpha})$, $k = 1, \dots, \frac{n}{2} + 1$;
- (iii) Compute $\mathbf{x} = \mathbf{U}_{\perp} \mathbf{C} + (\mathbf{I}_n - \mathbf{U}_{\perp} \mathbf{U}_{\perp}^{\top}) \mathcal{F}^{-1}(\tilde{\mathbf{x}})$.

Here, $i \in \mathbb{C}$ is the imaginary unit and $\mathcal{F}^{-1}: \mathbb{C}^{\frac{n}{2}+1} \rightarrow \mathbb{R}^n$ denotes the inverse of the real fast Fourier transform, implemented under `rfft` in the FFTW library [Frigo and Johnson, 1998]. Figure 4 shows six samples \mathbf{x} from this distribution.

We consider a Gaussian linear invariant-preserving process noise with zero mean and covariance $\sigma_{\mathbf{w}_t}^2 \mathbf{I}_n$ with $\sigma_{\mathbf{w}_t} = 10^{-2}$. The time step size between two assimilation cycles is $\Delta t_{\text{obs}} = 2 \cdot 10^{-1}$ (corresponding to half the convective time $t_c = L/c$, where L is the length of the domain Ω). We have incoming point observations at every fourth grid point ($d = 32$) corrupted by an additive zero-mean Gaussian noise with covariance $\sigma_{\boldsymbol{\varepsilon}}^2 \mathbf{I}_d$ with $\sigma_{\boldsymbol{\varepsilon}} = 10^{-1}$. The true mass \mathbf{C} is drawn from a Gaussian distribution with mean 1.0 and standard deviation $5 \cdot 10^{-2}$.

Figure 5 reports the time-averaged evolution of the RMSE and the spread of the linear advection problem using the UnEnKF (blue) and the ConsEnKF (yellow) for varying ensemble sizes M . Both filters use optimally tuned inflation and covariance tapering. We note that the ConsEnKF has a slightly better RMSE than its unconstrained version. This result is consistent with the results of Section 8.2 for small ratio r/n . The spread over the ensemble size is roughly similar. While these global metrics can be somewhat deceptive in terms of improvement, the true benefit of preserving the mass is revealed by examining the evolution of the mass estimate, which is reported in Figure 6.

We observe from Figure 6 that the ConsEnKF conserves mass up to machine precision. At the same time, the optimally tuned UnEnKF shows notable unphysical variations in the mass estimate (up to 20%) for $M = 40$ and does not necessarily converge to the true invariant as we assimilate more observations.

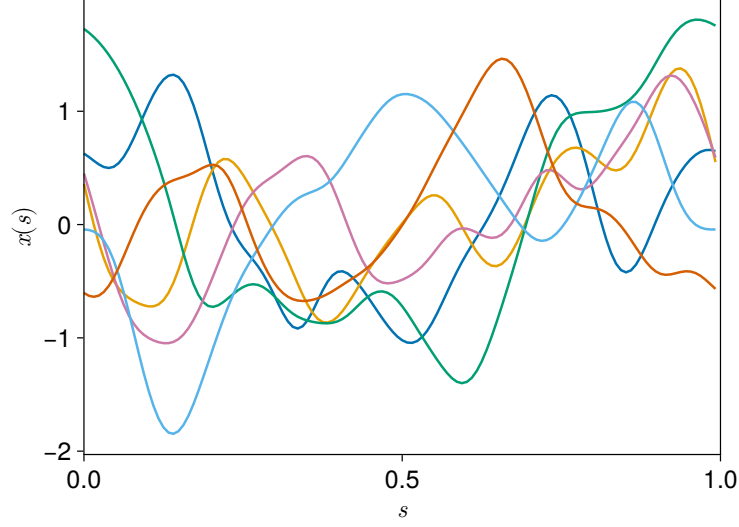


Figure 4: Six samples drawn from the distribution $\mathcal{S}_{n,r}(\mathbf{U}_\perp, \mathbf{C}, \alpha)$ with $n = 128$, $r = 1$, $\mathbf{U}_\perp = \mathbf{1}/n \in \mathbb{R}^n$, $\mathbf{C} = \mathbf{1} \in \mathbb{R}$, and $\alpha = 1$. The linear constraint for each sample is $\mathbf{U}_\perp^\top \mathbf{x} = 1$.

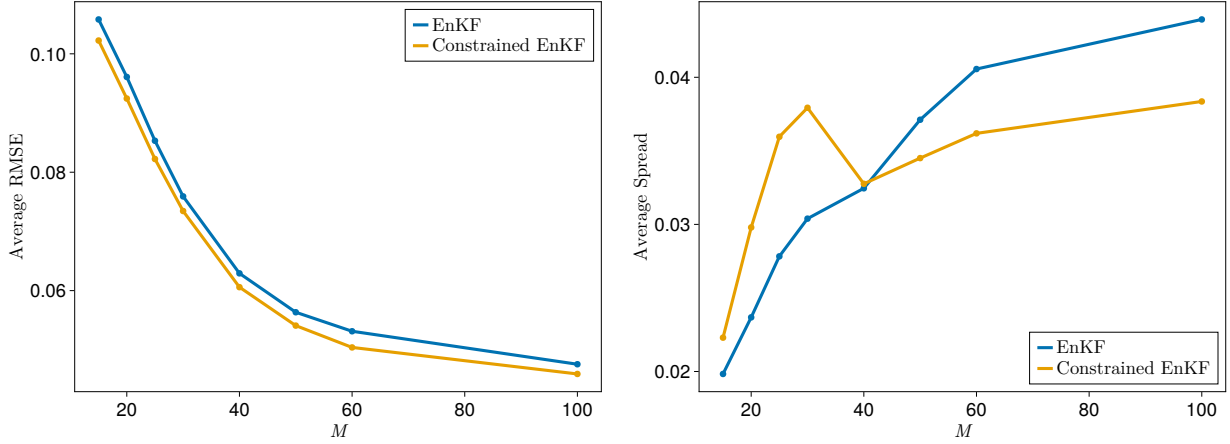


Figure 5: Left panel: Time-averaged evolution of the RMSE of the linear advection problem using the UnEnKF (blue) and the ConsEnKF (yellow) for varying ensemble sizes M . Right panel: Median evolution of the spread for varying ensemble sizes M . Both filters use optimally tuned inflation and covariance tapering.

8.4 A embedded Lorenz-63 model with a linear invariant

The Lorenz-63 model is a three-dimensional model for the atmospheric convection [Lorenz, 1963], used as a classical benchmark in data assimilation [Asch et al., 2016]. The state $\tilde{\mathbf{x}} = [\tilde{x}_1, \tilde{x}_2, \tilde{x}_3]^\top \in \mathbb{R}^3$ is governed by the following set of ODEs:

$$\frac{d\tilde{\mathbf{x}}}{dt} = \tilde{\mathfrak{F}}(\tilde{\mathbf{x}}, t) = \begin{bmatrix} \sigma(\tilde{x}_2 - \tilde{x}_1) \\ \tilde{x}_1(\rho - \tilde{x}_2) - \tilde{x}_2 \\ \tilde{x}_1\tilde{x}_2 - \beta\tilde{x}_3 \end{bmatrix}, \quad (40)$$

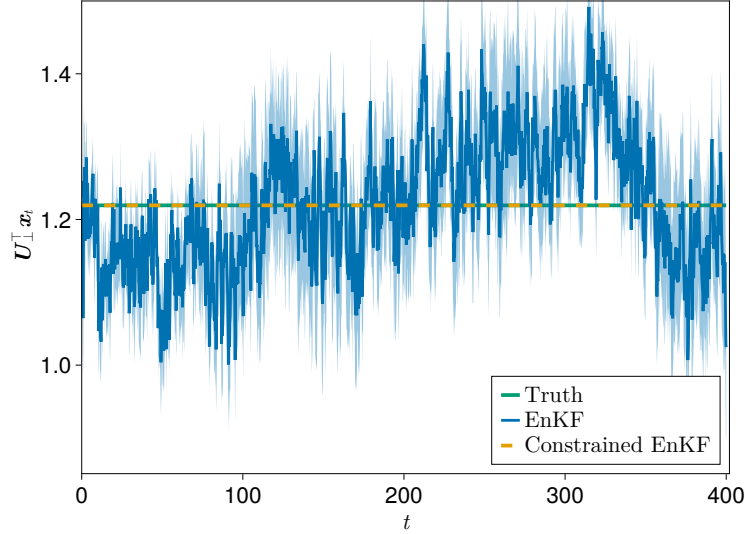


Figure 6: Time evolution of the linear invariant $U_{\perp}^T \mathbf{x}_t$ for the true state process (green) and the posterior mean obtained with the UnEnKF (blue) and the ConsEnKF (dashed yellow) for an ensemble size of $M = 40$. Faded areas show the 10% and 90% quantiles of the posterior estimate of the invariant. Both filters use optimally tuned inflation and covariance tapering.

where $\tilde{\mathfrak{F}}: \mathbb{R}^3 \times \mathbb{R} \rightarrow \mathbb{R}^3$ denotes the forward operator of (40), and σ, β, ρ are fixed parameters. In our simulation, we use $\sigma = 10, \beta = 8/3, \rho = 28$. For these values, the system is chaotic and behaves like a strange attractor [Lorenz, 1963]. We introduce an embedded version of the Lorenz-63 model with a linear invariant, called the embedded Lorenz-63 model. For this low-dimensional problem, covariance tapering or localization are not useful to regularize the unconstrained EnKF. Assuming that the linear invariant is constant over the forecast distribution $\pi_{\mathbf{x}_t | \mathbf{y}_{1:t-1}}$, Section 7 proves that in this case, the unconstrained EnKF preserves linear invariants. This example allows us to investigate the influence of a nonlinear analysis map and the preservation of linear invariants. We compare the constrained stochastic map filter (ConsSMF) with the unconstrained ensemble Kalman filter (UnEnKF) and stochastic map filter (UnSMF). Algorithm 1 in Appendix D provides a pseudo-code for the constrained SMF.

To construct the embedded Lorenz-63 model, we augment the state $\tilde{\mathbf{x}} \in \mathbb{R}^3$ of the original Lorenz-63 model of (40) by adding a fourth component \tilde{x}_4 with zero dynamics, i.e., $d\tilde{x}_4/dt = 0$, and performing a random rotation of the embedded coordinates. This random rotation allows us to create a dynamical system with a non-local linear invariant, i.e., the invariant depends on all the state variables. We denote the augmented state by $\tilde{\mathbf{x}}_{\text{aug}} \in \mathbb{R}^4$ and the augmented forward operator by $\tilde{\mathfrak{F}}_{\text{aug}}: \mathbb{R}^4 \times \mathbb{R} \rightarrow \mathbb{R}^4$, $(\tilde{\mathbf{x}}_{\text{aug}}, t) \mapsto [\tilde{\mathfrak{F}}(\tilde{\mathbf{x}}, t), 0]^T$. Observe that $\tilde{\mathbf{x}} \mapsto \tilde{U}_{\perp}^T \tilde{\mathbf{x}}$ is a linear invariant for the augmented state $\tilde{\mathbf{x}}$ with $\tilde{U}_{\perp} = [0, 0, 0, 1]^T$. We then apply a random orthogonal matrix $\mathbf{Q} \in \mathbb{R}^{4 \times 4}$ to $\tilde{\mathbf{x}}_{\text{aug}}$ to define the new state $\mathbf{x} = \mathbf{Q}\tilde{\mathbf{x}}_{\text{aug}}$. Thus, the state \mathbf{x} is governed by the ODE system

$$\frac{d\mathbf{x}}{dt} = \frac{d\mathbf{Q}\tilde{\mathbf{x}}_{\text{aug}}}{dt} = \mathbf{Q}\tilde{\mathfrak{F}}_{\text{aug}}(\mathbf{Q}^{-1}\mathbf{x}, t) = \mathbf{Q}\tilde{\mathfrak{F}}_{\text{aug}}(\mathbf{Q}^T\mathbf{x}, t), \quad (41)$$

where the last equality is due to the orthonormality of \mathbf{Q} . One can verify that the linear invariant $\mathbf{x} \mapsto \mathbf{U}_\perp^\top \mathbf{x}$ with $\mathbf{U}_\perp = \mathbf{Q}\tilde{\mathbf{U}}_\perp \in \mathbb{R}^4$ is preserved by (41):

$$\begin{aligned}
 \frac{d\mathbf{U}_\perp^\top \mathbf{x}}{dt} &= \tilde{\mathbf{U}}_\perp^\top \mathbf{Q}^\top \frac{d\mathbf{x}}{dt} \\
 &= \tilde{\mathbf{U}}_\perp^\top \mathbf{Q}^\top \mathbf{Q} \tilde{\mathfrak{F}}_{\text{aug}}(\mathbf{Q}^\top \mathbf{x}, t) \\
 &= \tilde{\mathbf{U}}_\perp^\top \tilde{\mathfrak{F}}_{\text{aug}}(\mathbf{Q}^\top \mathbf{x}, t) \\
 &= \langle [0, 0, 0, 1], [\tilde{\mathfrak{F}}(\mathbf{Q}^\top \mathbf{x}, t), 0] \rangle \\
 &= 0,
 \end{aligned} \tag{42}$$

where $\langle \cdot, \cdot \rangle$ denotes the Euclidian scalar product in \mathbb{R}^n . The random orthogonal rotation $\mathbf{Q} \in \mathbb{R}^{4 \times 4}$ is constructed by extracting the Q factor of the QR factorization of a 4×4 matrix whose entries are drawn from the standard Gaussian distribution. To solve (41), we use a fourth-order RK time integration scheme [Rackauckas and Nie, 2017]. The time step size between two assimilation cycles is $\Delta t_{\text{obs}} = 5 \cdot 10^{-2}$. We observe every component of the state, i.e., $d = n = 4$, corrupted by additive Gaussian observation noise with zero mean and covariance $\sigma_\varepsilon^2 \mathbf{I}_d$ with $\sigma_\varepsilon = 10^{-2}$. The initial distribution $\pi_{\mathbf{x}_0}$ is the standard Gaussian one. The true invariant \mathbf{C} is set to 1.

In the case of conditionally independent observations, i.e., if the likelihood factorizes as $\pi_{\mathbf{y} | \mathbf{x}} = \prod_{j=1}^d \pi_{y_j | \mathbf{x}}$, it is equivalent to assimilate a d -dimensional observation $\mathbf{y}^* \in \mathbb{R}^d$ at once, or to assimilate the observation components $y_j^* \in \mathbb{R}$, $j = 1, \dots, d$, in d recursive updates. We provide a justification in Appendix B. Thus, the analysis step can be equivalently performed by computing d analysis maps with $n + 1$ inputs—each map associated with one observation, or computing a single map with $d + n$ inputs. In practice, the number of samples to estimate the analysis map is small compared to the dimensions of the states and observations. Thus, to reduce the variance of the resulting analysis map \mathbf{T}_{y^*} , it is favorable to estimate d transport maps $\mathbf{S}^{\mathcal{X}}$ of $n + 1$ inputs rather than a single map $\mathbf{S}^{\mathcal{X}}$ of $d + n$ inputs. See [Spantini et al., 2022, Houtekamer and Mitchell, 2001] for further discussions. Following [Spantini et al., 2022], we apply the unconstrained/constrained stochastic map filters sequentially. To allow for a fair comparison, the unconstrained EnKF is also applied sequentially in this example.

Figure 7 reports the time-averaged evolution of the RMSE and the spread of the embedded Lorenz-63 model using the UnEnKF (blue), the UnSMF (yellow), and the ConsSMF (green) for varying ensemble sizes M . All filters have optimally tuned inflation. For small ensemble size $M < 100$, the unconstrained EnKF has a lower RMSE and spread than the stochastic map filters. For larger ensemble size $M > 100$, we observe a consistent improvement in the RMSE and spread with the nonlinear filters. For large ensemble size $M \approx 500$, the UnSMF and ConsSMF perform similarly in terms of RMSE and spread, corresponding to a reduction of the RMSE by 18% and the spread by 16% with respect to the EnKF. These results echo the conclusions of [Spantini et al., 2022] on the bias-variance tradeoff of nonlinear filters with limited samples. Interestingly, the ConsSMF always performs better than the UnSMF. For $M > 80$, the ConsSMF achieves the lowest RMSE and spread. For $M \in [60, 200]$, we observe that the RMSE of the ConsSMF rapidly decreases from $8.0 \cdot 10^{-1}$ for $M = 60$ to $5.3 \cdot 10^{-1}$ for $M = 200$. In contrast, the RMSE and spread of UnSMF have a slower decay with the ensemble size. The RMSE of the ConsSMF plateaus at about $5.3 \cdot 10^{-1}$ for $M > 160$, while the unconstrained SMF requires $M = 500$ samples to achieve a similar performance.

We observe from Figure 8 that the UnEnKF and the ConsSMF conserve the linear invariant. However, the UnSMF shows important variations in the linear invariant estimate (up to 200%) for $M = 160$. These results suggest that

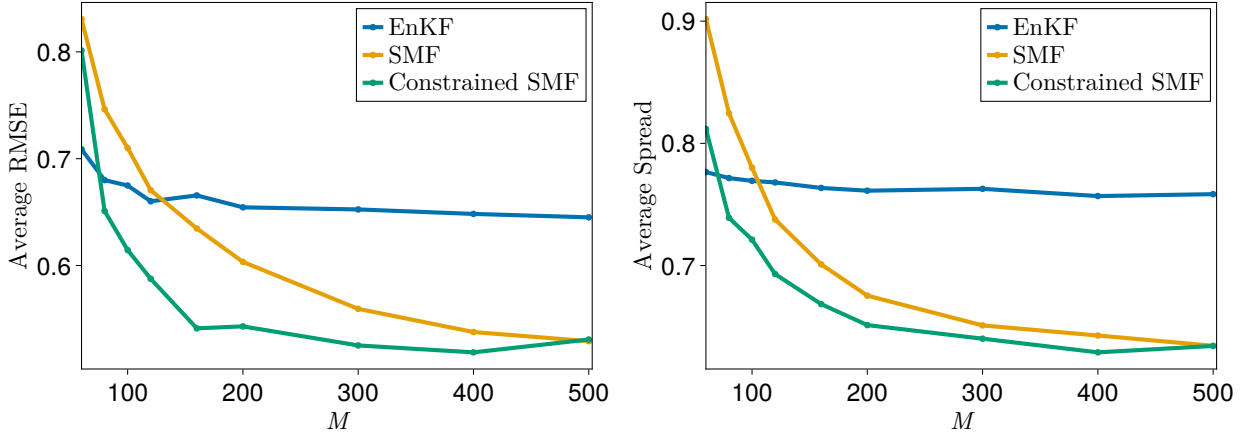


Figure 7: Left panel: Time-averaged evolution of the RMSE of the embedded Lorenz-63 model problem using the UnEnKF (blue), the UnSMF (yellow), and the ConsSMF (green) for varying ensemble sizes M . Right panel: Median evolution of the spread for varying ensemble sizes M . All filters use optimally tuned inflation.

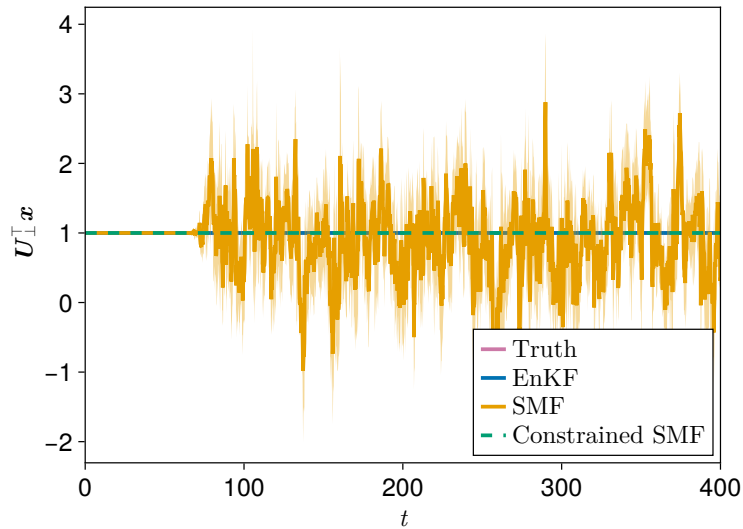


Figure 8: Time evolution of the linear invariant $U_{\perp}^T x_t$ for the true state process (pink) and the posterior mean obtained with the UnEnKF (blue), the unconstrained SMF (yellow), and the constrained SMF (dashed green) for an ensemble size of $M = 160$. Faded areas show the 10% and 90% quantiles of the posterior estimate of the invariant. All filters use optimally tuned inflation.

it is beneficial to combine the preservation of linear invariants with nonlinear prior-to-posterior transformations for non-Gaussian filtering problems.

9 Conclusion

We introduced a class of analysis maps (Lin-PAMs) that preserve linear invariants of the forecast distribution in non-Gaussian filtering problems. Linear invariants are found across a spectrum of problems in science and engineering,

including divergence-free conditions in incompressible fluid mechanics, conservation of electrical intensities and currents in Kirchhoff’s laws, and stoichiometric balance of chemical species in chemical reactions. To construct the proposed Lin-PAMs, we operate in two steps. First, we rotate the state coordinates such that the first state components align with the column space of U_{\perp} and the remaining state components span the orthogonal complement of U_{\perp} , i.e., $\text{span}(U_{\parallel})$. In this rotated space, the linear invariants are given by the first rotated state components, while the remaining state components do not influence the linear invariants. Thus, we can perform the same inference as in the original space by first rotating the state variables, then performing the inference for the first state components followed by the remaining ones, and finally lifting the result to the original space.

Essentially, we are operating a change of variables for the analysis map between the original and the rotated space. Second, we construct linear invariant-preserving analysis maps (Lin-PAMs) by omitting the update of the first state components corresponding to the linear invariants.

This formulation allows preserving linear invariants in non-Gaussian settings. By specializing this construction to a jointly Gaussian distribution for the observations and states, our formulation recovers a constrained formulation of the analysis map of the Kalman filter where the update is projected on the orthogonal complement of the columns of U_{\perp} . Then, we clarified existing results on preserving linear invariants for the vanilla (unconstrained) Kalman filter and ensemble Kalman filter. In particular, we show that regularization techniques for the ensemble Kalman filter, such as covariance inflation, localization, or tapering can violate linear invariants. We also show how to combine these regularization techniques for the ensemble Kalman filter with the preservation of the linear invariants.

We emphasize that the tools developed in this study are not limited to the filtering setting, as the analysis step essentially solves a static Bayesian inverse problem [Le Provost et al., 2021, 2022]. In fact, the techniques presented in this work are readily applicable to other ensemble-based methods used to solve static inverse problems while preserving linear invariants [Iglesias et al., 2013, Zhang et al., 2020, Garbuno-Inigo et al., 2020].

This work focused on the strong preservation of linear invariants in non-Gaussian settings. In future work, we will explore a variational formulation of Bayes’ rule [Sanz-Alonso et al., 2023] to preserve invariants in the weak sense for non-Gaussian settings.

More broadly, preserving invariants of the underlying dynamical models is critical for ensuring that the recent advances in Bayesian statistics produce posterior estimates respecting our fundamental knowledge of physics. In future work, we plan to construct analysis maps and resulting ensemble filters for important non-linear invariants, such as Hamiltonians in mechanics [del Castillo, 2018] or energy and entropy in hyperbolic conservation laws [LeVeque, 1992]. It would also be interesting to consider a weak preservation of non-linear invariants in non-Gaussian settings. In future work, we plan to exploit a variational formulation of Bayes’ rule [Trillos and Sanz-Alonso, 2018, Sanz-Alonso et al., 2023] to tackle this problem.

Data Accessibility: All the computational results are reproducible, and code is available at <https://github.com/mleprovost/Paper-Linear-Invariants-Ensemble-Filters>.

Authors’ Contributions: MLP: Conceptualization, Writing - Original Draft, Review & Editing, Software. JG: Conceptualization, Writing - Review & Editing. YM: Conceptualization, Writing - Review & Editing. The final version of the manuscript was approved by all authors.

Funding: MLP and YM acknowledge support of the National Science Foundation under Grant PHY-2028125. JG and YM acknowledge support of the US DOD (ONR MURI) under Grant N00014-20-1-2595.

Acknowledgements: The authors would like to thank Ricardo Baptista, Jeff Eldredge, Thomas Izgin, Matthew Levine, and Daniel Sharp for insightful discussions and constructive feedback.

Appendix

A A result on the preservation of invariants in Bayesian inference problems

Theorem 1. Consider a prior distribution $\pi_{\mathbf{X}}$, a likelihood model $\pi_{\mathbf{Y}|\mathbf{X}}$, and an invariant $\mathbf{H}: \mathbb{R}^n \rightarrow \mathbb{R}^r$. Let us assume that the invariant \mathbf{H} is constant over the prior distribution $\pi_{\mathbf{X}}$, i.e., $\mathbf{H}(\mathbf{x}) = \mathbf{C} \in \mathbb{R}^r$ for any realization \mathbf{x} of \mathbf{X} . Then the invariant \mathbf{H} is also constant over the posterior distribution $\pi_{\mathbf{X}|\mathbf{Y}}$.

Proof. For a distribution π , its support is defined as $\text{supp}(\pi) = \{\mathbf{x} \in \mathbb{R}^n | \pi(\mathbf{x}) > 0\}$. If the invariant \mathbf{H} is constant over the prior distribution $\pi_{\mathbf{X}}$, then

$$\text{supp}(\pi_{\mathbf{X}}) \subseteq \{\mathbf{x} \in \mathbb{R}^n | \mathbf{H}(\mathbf{x}) = \mathbf{C}\}. \quad (43)$$

For a likelihood model $\pi_{\mathbf{Y}|\mathbf{X}}$, we have from Bayes' rule that the support of the posterior $\pi_{\mathbf{X}|\mathbf{Y}} = \pi_{\mathbf{Y}|\mathbf{X}} \cdot \pi_{\mathbf{X}} / \pi_{\mathbf{Y}}$ is included in the support of the prior $\pi_{\mathbf{X}}$, i.e.,

$$\text{supp}(\pi_{\mathbf{X}|\mathbf{Y}}) \subseteq \text{supp}(\pi_{\mathbf{X}}). \quad (44)$$

Indeed, a multiplication by the non-negative quantity $\pi_{\mathbf{Y}|\mathbf{X}}(\mathbf{y}|\mathbf{x})/\pi_{\mathbf{Y}}(\mathbf{y}) \geq 0$ cannot increase the posterior support $\text{supp}(\pi_{\mathbf{X}|\mathbf{Y}})$ beyond the prior support $\text{supp}(\pi_{\mathbf{X}})$. Combining (43) and (44), we conclude that

$$\text{supp}(\pi_{\mathbf{X}|\mathbf{Y}}) \subseteq \{\mathbf{x} \in \mathbb{R}^n | \mathbf{H}(\mathbf{x}) = \mathbf{C}\}. \quad (45)$$

□

B Recursive assimilation of conditionally independent observations

In many settings, the observations $\mathbf{Y} \in \mathbb{R}^d$ to assimilate are conditionally independent, i.e., $Y_j \perp\!\!\!\perp Y_k | \mathbf{X}$ for $j \neq k$, [Spantini et al., 2022, Houtekamer and Mitchell, 2001]. Then the likelihood $\pi_{\mathbf{Y}|\mathbf{X}}$ factorizes as

$$\pi_{\mathbf{Y}|\mathbf{X}} = \prod_{j=1}^d \pi_{Y_j|\mathbf{X}}. \quad (46)$$

In this case, we will show that the assimilation of a d -dimensional observation $\mathbf{y}^* \in \mathbb{R}^d$ can be made in d recursive steps by assimilating one scalar observation y_j^* at a time in the state, i.e., the posterior from assimilating j components $\mathbf{y}_{1:j}^*$ can be used as a prior for assimilating the next scalar observation y_{j+1}^* . From Bayes' rule, we derive a recursive relation to assimilate the observation Y_{j+1} in the conditional distribution $\pi_{\mathbf{X}|\mathbf{Y}_{1:j}}$:

$$\pi_{\mathbf{X}|\mathbf{Y}_{1:j+1}} = \frac{\pi_{Y_{j+1}|\mathbf{X}} \pi_{\mathbf{X}}}{\pi_{Y_{j+1}}} = \frac{\pi_{Y_{j+1}|\mathbf{X}, \mathbf{Y}_{1:j}} \pi_{Y_{1:j}|\mathbf{X}} \pi_{\mathbf{X}}}{\pi_{Y_{j+1}|\mathbf{Y}_{1:j}} \pi_{Y_{1:j}}} = \frac{\pi_{Y_{j+1}|\mathbf{X}, \mathbf{Y}_{1:j}}}{\pi_{Y_{j+1}|\mathbf{Y}_{1:j}}} \pi_{\mathbf{X}|\mathbf{Y}_{1:j}}. \quad (47)$$

This factorization holds for an arbitrary likelihood $\pi_{\mathbf{Y}|\mathbf{X}}$. In general, the ‘‘conditional’’ likelihood $\pi_{\mathbf{Y}_{j+1}|\mathbf{X},\mathbf{Y}_{1:j}}$ is intractable, and one cannot easily use (47) to perform a recursive update of the prior without further assumptions on the likelihood $\pi_{\mathbf{Y}|\mathbf{X}}$. However, if we assume that the observations are conditionally independent, i.e., $Y_j \perp\!\!\!\perp Y_k | \mathbf{X}$ for $j \neq k$, (47) simplifies to

$$\pi_{\mathbf{X}|\mathbf{Y}_{1:j+1}} = \frac{\pi_{\mathbf{Y}_{j+1}|\mathbf{X}}}{\pi_{\mathbf{Y}_j}} \pi_{\mathbf{X}|\mathbf{Y}_{1:j}}, \quad (48)$$

and one can assimilate the observations in a recursive manner.

C Details on the parameterization of the stochastic map filter

This section provides a summary of the parameterization of the Knothe-Rosenblatt rearrangement used in the unconstrained/constrained stochastic map filters. See [Spantini et al., 2022] for further details. Let $\mathbf{X} \in \mathbb{R}^n$ be a random variable with distribution π , and $\mathcal{S}: \mathbb{R}^n \rightarrow \mathbb{R}^n$ be the Knothe-Rosenblatt rearrangement that pushes forward π to the reference distribution η . We consider a linearly separable parameterization for the components $\{S^k\}$ of \mathcal{S} , i.e., the k th map component $S^k: \mathbb{R}^k \rightarrow \mathbb{R}$ is parameterized by

$$S^k(\mathbf{x}_{1:k}) = \sum_{j=1}^{k-1} \varphi^{(j,k)}(x_j) + \varphi^{(k,k)}(x_k), \quad (49)$$

where $\varphi^{(j,k)}: \mathbb{R} \rightarrow \mathbb{R}, j = 1, \dots, k$ are univariate feature functions. Each off-diagonal feature $\varphi^{(j,k)}$, i.e., with index $j < k$, is given by the sum of a linear term and p radial basis functions characterized by their centers $\xi_j = [\xi_j^{(1)}, \dots, \xi_j^{(p)}]^\top \in \mathbb{R}^p$ and scale widths $\sigma_j = [\sigma_j^{(1)}, \dots, \sigma_j^{(p)}]^\top \in \mathbb{R}^p$, i.e.,

$$\varphi^{(j,k)}(x_j) = c_{j,0}x_j + \sum_{l=1}^p c_{j,l} \mathcal{N}\left(\xi_j^{(l)}, \sigma_j^{(l)}\right)(x_j), \quad (50)$$

where $\mathcal{N}\left(\xi_j^{(l)}, \sigma_j^{(l)}\right)(x_j)$ denotes the evaluation of the univariate Gaussian distribution with mean $\xi_j^{(l)}$ and standard deviation $\sigma_j^{(l)}$ at x_j . The coefficients $\{c_{j,l}\}$ are unknown and estimated from samples. The centers ξ_j are identified as the p empirical quantiles of the j th component of the samples. The scale widths σ_j quantifying the empirical spread in the j th component, are defined as $\sigma_j^{(l)} = \gamma(\xi_{j+1} - \xi_{j-1})/2$ with scaling factor $\gamma > 0$, $\xi_0 = \xi_1$ and $\xi_{p+1} = \xi_p$. We set $\gamma = 2.0$ in our numerical experiments. For $p = 0$, the off-diagonal feature $\varphi^{(j,k)}$ reverts to a linear function. To enforce the monotonicity constraint on the map component S^k , i.e., $x \mapsto S^k(\mathbf{x}_{1:k-1}, x)$ is strictly increasing for all $\mathbf{x}_{1:k-1} \in \mathbb{R}^{k-1}$, the diagonal feature $\varphi^{(k,k)}$ is decomposed as a non-negative sum of a constant $c_{k,0}$ and $p + 2$ strictly increasing functions $\{\psi^{(l)}: \mathbb{R} \rightarrow \mathbb{R}\}$, i.e.,

$$\varphi^{(k,k)}(x_k) = c_{k,0} + \sum_{l=1}^{p+2} c_{k,l} \psi^{(l)}(x_k), \quad (51)$$

where the $p + 2$ functions $\{\psi^{(l)}\}$ are parameterized by a center parameter $\xi_k^{(l)}$, a width parameter $\sigma_k^{(l)}$, and given by

$$\begin{aligned} \psi^{(1)}(z) &= \frac{1}{2} \left(\left(z - \xi_k^{(1)} \right) \left(1 - \operatorname{erf} \left(\Delta_k^{(1)} \right) \right) - \sigma_k^{(1)} \sqrt{2/\pi} \exp \left(- \left(\Delta_k^{(1)} \right)^2 \right) \right), \\ \psi^{(l)}(z) &= \frac{1}{2} \left(1 + \operatorname{erf} \left(\Delta_k^{(l)} \right) \right), \text{ for } l = 2, \dots, p + 1, \\ \psi^{(p+2)} &= \frac{1}{2} \left(\left(z - \xi_k^{(p+1)} \right) \left(1 + \operatorname{erf} \left(\Delta_k^{(p+1)} \right) \right) + \sigma_k^{(p+1)} \sqrt{2/\pi} \exp \left(- \left(\Delta_k^{(p+1)} \right)^2 \right) \right), \end{aligned} \quad (52)$$

where $\Delta_k^{(l)}(x_k) = (x_k - \xi_k^{(l)})/\sqrt{2}\sigma_k^{(l)}$ for $l = 1, \dots, p+2$. The identification of the set of $p+2$ centers $\xi_k = [\xi_k^{(0)}, \dots, \xi_k^{(p+1)}]^\top \in \mathbb{R}^{p+2}$ and scale widths $\sigma_k = [\sigma_k^{(0)}, \dots, \sigma_k^{(p+1)}]^\top \in \mathbb{R}^{p+2}$ follow the same procedure as for the off-diagonal features $\varphi^{(j,k)}$. The strict monotonicity of S^k is then enforced by the positivity constraints: $c_{k,l} \geq 0$ for $l = 0, \dots, p+2$. For $p = 0$, we set $\varphi^{(k,k)}$ to be a strictly increasing affine function, i.e., $\varphi^{(k,k)}(x_k) = c_{k,0} + c_{k,1}x_k$ with $c_{k,1} > 0$. The resulting parameterization of the map components concentrates nonlinear features in the bulk of the joint forecast distribution, and reverts to a linear behavior in the tails of the joint forecast for robustness.

In this work, we consider further simplifications of the parameterization. For $k > 2$, the off-diagonal features are given by a linear term plus p radial basis functions, while the diagonal feature $\varphi^{(k,k)}$ is affine. For $k = 1, 2$, the diagonal feature $\varphi^{(k,k)}$ is given by a constant plus $p+2$ increasing functions $\{\psi^{(l)}: \mathbb{R} \rightarrow \mathbb{R}\}$ given by (52). In our experiments, we use $p = 2$. For $k > 2$, one can exploit this parameterization and solve in closed form for the coefficients $c_{l,j}$ by solving a least square problem [Spantini et al., 2022]. For $k = 1, 2$, the optimization of the coefficients is performed with a projected Newton's method [Bertsekas, 1982]. We note that the optimization of the first map component S^1 can be skipped. Indeed, the analysis map (8) only depends on the lower map $S^{\mathcal{X}}$. The upper map $S^{\mathcal{Y}}$ is only an artifact of construction of the analysis map [Spantini et al., 2022, Le Provost et al., 2023]. We refer readers to [Spantini et al., 2022] for details on the estimation of the coefficients of the map components from samples.

D Algorithm for the analysis step of the constrained stochastic map filter

Algorithm 1 presents pseudo-code for one analysis step of the constrained stochastic map filter (ConsSMF). This algorithm transforms a set of forecast samples to filtering samples by assimilating the realization \mathbf{y}^* of the observation variable while preserving linear invariants of the samples.

Algorithm 1: ConsSMF($\mathbf{y}^*, \pi_{\mathbf{Y}|\mathbf{X}=\cdot}, \{\mathbf{x}^i\}$) assimilates the data \mathbf{y}^* in the prior samples $\{\mathbf{x}^1, \dots, \mathbf{x}^M\}$ while preserving the linear invariants of the samples.

Input: $\mathbf{y}^* \in \mathbb{R}^d$, likelihood model $\pi_{\mathbf{Y}|\mathbf{X}=\cdot}$, M samples $\{\mathbf{x}^i\}$ from $\pi_{\mathbf{X}}$

Output: M samples $\{\mathbf{x}_a^{(i)}\}$ from $\pi_{\mathbf{X}|\mathbf{Y}=\mathbf{y}^*}$

```

/* Generate likelihood samples  $\{\mathbf{y}^{(i)}\}$  */
1 for  $\underline{= 1} : M$  do
2   Draw sample  $\mathbf{y}^{(i)}$  from  $\pi_{\mathbf{Y}|\mathbf{X}=\mathbf{x}^{(i)}}$ 
   /* Project the forecast samples  $\{\mathbf{x}^{(i)}\}$  onto  $\mathbf{U}_\perp$  and  $\mathbf{U}_\parallel$  : */
3    $\mathbf{x}_\perp^{(i)} = \mathbf{U}_\perp^\top \mathbf{x}^{(i)}$ ,  $\mathbf{x}_\parallel^{(i)} = \mathbf{U}_\parallel^\top \mathbf{x}^{(i)}$ 
4   Estimate the transport map  $S^{\mathcal{X}\parallel}$  from the transformed joint samples  $\{(\mathbf{y}^{(i)}, \mathbf{x}_\perp^{(i)}, \mathbf{x}_\parallel^{(i)})\}$ 
   /* Perform the constrained analysis in the transformed space by partial inversion of  $S^{\mathcal{X}\parallel}$  : */
5    $\mathbf{x}_{\parallel,a}^{(i)} = \tilde{T}_{\mathbf{y}^*}^\parallel(\mathbf{y}^{(i)}, \mathbf{x}_\perp^{(i)}, \mathbf{x}_\parallel^{(i)}) = S^{\mathcal{X}\parallel}(\mathbf{y}^*, \mathbf{x}_\perp^{(i)}, \cdot)^{-1} \circ S^{\mathcal{X}\parallel}(\mathbf{y}^{(i)}, \mathbf{x}_\perp^{(i)}, \mathbf{x}_\parallel^{(i)})$ 
   /* Lift result to the original space: */
6    $\mathbf{x}_a^{(i)} = \mathbf{U}_\perp \mathbf{x}_\perp^{(i)} + \mathbf{U}_\parallel \mathbf{x}_{\parallel,a}^{(i)}$ 
7 return  $\{\mathbf{x}_a^i\}$ 

```

E Algorithm for the analysis step of the constrained ensemble Kalman filter

Algorithm 2 presents pseudo-code for one analysis step of the constrained ensemble Kalman filter (ConsEnKF). This algorithm transforms a set of forecast samples to filtering samples by assimilating the realization \mathbf{y}^* of the observation variable while preserving linear invariants $\mathbf{U}_\perp^\top \mathbf{x} = \mathbf{C} \in \mathbb{R}^r$ of the samples .

Algorithm 2: ConsEnKF(\mathbf{y}^* , \mathbf{G} , $\pi_{\mathcal{E}}$, \mathbf{U}_\perp , $\{\mathbf{x}^i\}$) assimilates the data \mathbf{y}^* in the prior samples $\{\mathbf{x}^1, \dots, \mathbf{x}^M\}$ while preserving the linear invariants $\mathbf{U}_\perp^\top \mathbf{x} = \mathbf{C}$ of the samples.

Input: $\mathbf{y}^* \in \mathbb{R}^d$, linear observation operator $\mathbf{G} \in \mathbb{R}^{d \times n}$, observation noise distribution $\pi_{\mathcal{E}} = \mathcal{N}(\mathbf{0}_d, \Sigma_{\mathcal{E}})$, sub-unitary matrix $\mathbf{U}_\perp \in \mathbb{R}^{r \times n}$ for the linear invariants $\mathbf{U}_\perp^\top \mathbf{x} = \mathbf{C} \in \mathbb{R}^r$, M samples $\{\mathbf{x}^i\}$ from $\pi_{\mathbf{X}}$

Output: M samples $\{\mathbf{x}_a^{(i)}\}$ from $\pi_{\mathbf{X} | \mathbf{Y}=\mathbf{y}^*}$

```

/* Generate observation noise samples  $\{\epsilon^{(i)}\}$  from  $\mathcal{N}(\mathbf{0}_d, \Sigma_{\mathcal{E}})$  */
1 : for  $i = 1 : M$  do
2   Draw sample  $\epsilon^{(i)}$  from  $\mathcal{N}(\mathbf{0}_d, \Sigma_{\mathcal{E}})$ 
/* Form the perturbation matrices for the state  $\mathbf{A}_{\mathbf{X}} \in \mathbb{R}^{n \times M}$  and the observation noise
 $\mathbf{A}_{\mathcal{E}} \in \mathbb{R}^{d \times M}$ : */
3 for  $i = 1 : M$  do
4    $\mathbf{A}_{\mathbf{X}}[:, i] \leftarrow \frac{1}{\sqrt{M-1}} (\mathbf{x}^{(i)} - \hat{\boldsymbol{\mu}}_{\mathbf{X}})$ 
5    $\mathbf{A}_{\mathcal{E}}[:, i] \leftarrow \frac{1}{\sqrt{M-1}} (\epsilon^{(i)} - \hat{\boldsymbol{\mu}}_{\mathcal{E}})$ 
/* Apply the Kalman gain based on the representers [Burgers et al., 1998]. Solve the linear
system for  $\{\mathbf{b}^{(i)}\}$ : */
6 for  $i = 1 : M$  do
7    $((\mathbf{G}\mathbf{A}_{\mathbf{X}})(\mathbf{G}\mathbf{A}_{\mathbf{X}})^\top + \mathbf{A}_{\mathcal{E}}\mathbf{A}_{\mathcal{E}}^\top)\mathbf{b}^{(i)} = (\mathbf{G}\mathbf{x}^{(i)} + \epsilon^{(i)} - \mathbf{y}^*)$ ,
/* Build the posterior samples  $\{\mathbf{x}_a^{(i)}\}$ : */
8 for  $i = 1 : M$  do
9    $\mathbf{x}_a^{(i)} \leftarrow \mathbf{x}^{(i)} - (\mathbf{I}_n - \mathbf{U}_\perp\mathbf{U}_\perp^\top)\mathbf{A}_{\mathbf{X}}(\mathbf{G}\mathbf{A}_{\mathbf{X}})^\top\mathbf{b}^{(i)}$ .
10 return  $\{\mathbf{x}_a^i\}$ 

```

References

- D. J. Albers, P.-A. Blancquart, M. E. Levine, E. E. Seylabi, and A. Stuart. Ensemble Kalman Methods with Constraints. *Inverse Problems*, 35(9):095007, 2019.
- N. Amor, G. Rasool, and N. C. Bouaynaya. Constrained State Estimation – A Review. *arXiv preprint arXiv:1807.03463*, 2018.
- M. Asch, M. Bocquet, and M. Nodet. *Data assimilation: methods, algorithms, and applications*, volume 11. SIAM, 2016.
- R. Baptista, B. Hosseini, N. B. Kovachki, and Y. Marzouk. Conditional sampling with monotone GANs: from generative models to likelihood-free inference. *arXiv preprint arXiv:2006.06755*, 2020.

- T. Bengtsson, P. Bickel, and B. Li. Curse-of-Dimensionality Revisited: Collapse of the Particle Filter in Very Large Scale Systems. In Probability and Statistics: Essays in Honor of David A. Freedman, volume 2, pages 316–335. Institute of Mathematical Statistics, 2008.
- D. P. Bertsekas. Projected Newton methods for optimization problems with simple constraints. SIAM Journal on control and Optimization, 20(2):221–246, 1982.
- S. L. Brunton and J. N. Kutz. Data-Driven Science and Engineering: Machine Learning, Dynamical Systems, and Control. Cambridge University Press, 2019.
- G. Burgers, P. J. van Leeuwen, and G. Evensen. Analysis Scheme in the Ensemble Kalman Filter. Monthly Weather Review, 126(6), 1998.
- A. Carrassi, M. Bocquet, L. Bertino, and G. Evensen. Data assimilation in the geosciences: An overview of methods, issues, and perspectives. Wiley Interdisciplinary Reviews: Climate Change, 9(5):e535, 2018.
- C. Cotter, D. Crisan, D. Holm, W. Pan, and I. Shevchenko. Data assimilation for a quasi-geostrophic model with circulation-preserving stochastic transport noise. Journal of Statistical Physics, 179(5-6):1186–1221, 2020.
- R. R. Craig Jr and A. J. Kurdila. Fundamentals of structural dynamics. John Wiley & Sons, 2006.
- G. F. T. del Castillo. An Introduction to Hamiltonian Mechanics. Springer, 2018.
- G. Evensen. Sequential Data Assimilation with a Nonlinear Quasi-Geostrophic Model Using Monte Carlo Methods to Forecast Error Statistics. Journal of Geophysical Research: Oceans, 99(C5):10143–10162, 1994.
- G. Evensen, F. C. Vossepoel, and P. J. Van Leeuwen. Data assimilation fundamentals. Springer Nature, 2022.
- M. Frigo and S. G. Johnson. FFTW: An Adaptive Software Architecture for the FFT. In Proceedings of the 1998 IEEE International Conference on Acoustics, Speech and Signal Processing, ICASSP'98 (Cat. No. 98CH36181), volume 3, pages 1381–1384. IEEE, 1998.
- A. Garbuno-Inigo, F. Hoffmann, W. Li, and A. M. Stuart. Interacting Langevin diffusions: Gradient structure and ensemble Kalman sampler. SIAM Journal on Applied Dynamical Systems, 19(1):412–441, 2020.
- G. H. Golub and C. F. Van Loan. Matrix computations. JHU press, 2013.
- N. Gupta and R. Hauser. Kalman Filtering with Equality and Inequality State Constraints. arXiv preprint arXiv:0709.2791, 2007.
- E. Hairer, M. Hochbruck, A. Iserles, and C. Lubich. Geometric numerical integration. Oberwolfach Reports, 3(1): 805–882, 2006.
- P. L. Houtekamer and H. L. Mitchell. A sequential ensemble Kalman filter for atmospheric data assimilation. Monthly Weather Review, 129(1):123–137, 2001.
- J. Huang, T. Izgin, S. Kopecz, A. Meister, and C.-W. Shu. On the stability of strong-stability-preserving modified Patankar Runge-Kutta schemes. arXiv preprint arXiv:2205.01488, 2022.
- M. A. Iglesias, K. J. Law, and A. M. Stuart. Ensemble Kalman methods for inverse problems. Inverse Problems, 29(4): 045001, 2013.
- T. Izgin and P. Öffner. A study of the local dynamics of modified Patankar DeC and higher order modified Patankar–RK methods. ESAIM: Mathematical Modelling and Numerical Analysis, 57(4):2319–2348, 2023.

- T. Izgin, S. Kopecz, and A. Meister. A stability analysis of modified Patankar–Runge–Kutta methods for a nonlinear production–destruction system. PAMM, 22(1):e202200083, 2023.
- T. Janjić, D. McLaughlin, S. E. Cohn, and M. Verlaan. Conservation of mass and preservation of positivity with ensemble-type Kalman filter algorithms. Monthly Weather Review, 142(2):755–773, 2014.
- T. Kajishima, K. Takizawa, and M. Tsubokura. Computational Fluid Dynamics in Practice. CRC Press, 2016.
- R. E. Kalman. A New Approach to Linear Filtering and Prediction Problems. Journal of Basic Engineering, 82(1): 35–45, 03 1960.
- K. J. Law and A. M. Stuart. Data Assimilation: A Mathematical Introduction. Texts in Applied Mathematics, 62, 2015.
- M. Le Provost, R. Baptista, Y. Marzouk, and J. Eldredge. A low-rank nonlinear ensemble filter for vortex models of aerodynamic flows. In AIAA Scitech 2021 Forum, page 1937, 2021.
- M. Le Provost, R. Baptista, Y. Marzouk, and J. D. Eldredge. A low-rank ensemble Kalman filter for elliptic observations. Proceedings of the Royal Society A, 478(2266):20220182, 2022.
- M. Le Provost, R. Baptista, J. D. Eldredge, and Y. Marzouk. An adaptive ensemble filter for heavy-tailed distributions: tuning-free inflation and localization. arXiv preprint arXiv:2310.08741, 2023.
- R. J. LeVeque. Numerical methods for conservation laws, volume 214. Springer, 1992.
- E. Lorenz. Deterministic Nonperiodic Flow. Journal of Atmospheric Sciences, 20(2), 1963.
- Y. Marzouk, T. Moselhy, M. Parno, and A. Spantini. Sampling via measure transport: An introduction. Handbook of Uncertainty Quantification, 1:2, 2016.
- S. Nüßlein, H. Ranocha, and D. I. Ketcheson. Positivity-preserving adaptive Runge–Kutta methods. Communications in Applied Mathematics and Computational Science, 16(2):155–179, 2021.
- G. Peyré, M. Cuturi, et al. Computational optimal transport: With applications to data science. Foundations and Trends® in Machine Learning, 11(5-6):355–607, 2019.
- J. Prakash, S. C. Patwardhan, and S. L. Shah. Constrained nonlinear state estimation using ensemble Kalman filters. Industrial & Engineering Chemistry Research, 49(5):2242–2253, 2010.
- C. Rackauckas and Q. Nie. Differentialequations.jl – A performant and Feature-rich Ecosystem for Solving Differential Equations in Julia. Journal of open research software, 5(1):15–15, 2017.
- M. Ramgraber, R. Baptista, D. McLaughlin, and Y. Marzouk. Ensemble transport smoothing. Part I: Unified framework. Journal of Computational Physics: X, 17:100134, 2023.
- M. Rosenblatt. Remarks on a multivariate transformation. The Annals of Mathematical Statistics, 23(3):470–472, 1952.
- D. Sanz-Alonso, A. Stuart, and A. Taeb. Inverse Problems and Data Assimilation. London Mathematical Society Student Texts. Cambridge University Press, 2023.
- D. Simon. Kalman filtering with state constraints: a survey of linear and nonlinear algorithms. IET Control Theory & Applications, 4(8):1303–1318, 2010.
- C. Snyder, T. Bengtsson, P. Bickel, and J. Anderson. Obstacles to High-Dimensional Particle Filtering. Monthly Weather Review, 136(12):4629–4640, 2008.

- A. Spantini, R. Baptista, and Y. Marzouk. Coupling techniques for nonlinear ensemble filtering. SIAM Review, 64(4): 921–953, 2022.
- N. G. Trillos and D. Sanz-Alonso. The bayesian update: variational formulations and gradient flows. arXiv preprint arXiv:1705.07382, 2018.
- C. Villani et al. Optimal transport: Old and New, volume 338. Springer, 2009.
- J. Wu, J.-X. Wang, and S. C. Shadden. Adding constraints to Bayesian inverse problems. In Proceedings of the AAAI Conference on Artificial Intelligence, volume 33, pages 1666–1673, 2019.
- X.-L. Zhang, C. Michelén-Ströfer, and H. Xiao. Regularized ensemble Kalman methods for inverse problems. Journal of Computational Physics, 416:109517, 2020.